SEDIMENTOLOGY the journal of the International Association of Sedimentologists

*Sedimentology* (2021) **68**, 135–167 doi: 10.1111/sed.12789

# Autostratigraphic modelling of the growth of alluvial-shelf systems during steady base-level cycles: Two-dimensional tank experiments

JUNHUI WANG*,†,‡ and TETSUJI MUTO‡

**State Key Laboratory of Petroleum Resources and Prospecting, China University of Petroleum (Beijing), Beijing 102249, China (E-mail: wangjunhui@cup.edu.cn)*

*†College of Geosciences, China University of Petroleum (Beijing), Beijing 102249, China*

*‡Department of Environmental Science, Nagasaki University, Nagasaki 852-8521, Japan (E-mail: tmuto@nagasaki-u.ac.jp)*

Associate Editor – Kyle Straub

**ABSTRACT**

Autostratigraphy is the stratigraphy generated by large-scale autogenesis, developed based on the full recognition of the non-equilibrium behaviour of depositional systems in response to steady external forcing. The existing autostratigraphic concepts were derived mostly from studies of river deltas growing during a single rise or fall of base level (or relative sea level). The present study challenges to extend the autostratigraphic framework to the alluvial-shelf system growing through steady base-level cycles by two-dimensional tank experiments. During each experimental run, the base level was changed symmetrically, wherein through cycles, the rise and fall had the same constant rate ($|R_{bl}|$) and period ($T_{bl}$), and thus the same constant amplitude ($A_{bl}$), but with no basin tectonism. In total, nine runs with different combinations of $|R_{bl}|$ and $A_{bl}$ were performed. The experimental results brought the following implications. (i) The shelf-transiting active depositional system takes non-equilibrium responses in earlier base-level cycles, during each of which the system experiences episodes of degradation with base-level fall. (ii) After the system has sufficiently grown through cycles, non-equilibrium responses change into equilibrium responses, whereby the shelf-transiting alluvial system, whether retrogradational or progradational, is free from degradation and continues to aggrade but with a gradually decreasing rate of aggradation. (iii) The alluvial topset river tentatively but autogenically attains a graded state during the falling limb of an intermediate cycle, which separates the earlier degradation-inclusive and later aggradation-sustainable cycles. (iv) The number (or duration) of cycles elapsed prior to this phase-transition is linearly proportional to the amplitude (or the square of the period) of base-level cycles, with a coefficient defined by the rates of base-level change and sediment supply. Such a growth pattern does not necessarily hold when considering long-term tectonic subsidence or uplift. These notions help to understand the stratigraphic architectures of natural alluvial-shelf systems evolved through base level cycles.

**Keywords** Autostratigraphy, base-level cycle, deltaic shelf growth, grade, length and time scales, size effect, tank experiment.

## INTRODUCTION

The alluvial-shelf system, having the areal extent from a downstream alluvial realm (both deltaic and non-deltaic) to the distal end of a shelf floor, is a main component of the 'source to sink' profile (Burgess & Allen, 1996; Burgess *et al.*, 2008; Steel *et al.*, 2008; Helland-Hansen *et al.*, 2012; Patruno & Helland-Hansen, 2018). The stratigraphy of alluvial-shelf systems growing under base-level cycles (or relative sea-level cycles) has been developed through both physical experimentation (Paola *et al.*, 2001; Van Heijst & Postma, 2001; Kim *et al.*, 2006; Martin *et al.*, 2009; Yu *et al.*, 2017; Straub & Foreman, 2018; Straub, 2019) and numerical simulation (Burgess & Allen, 1996; Hoogendoorn *et al.*, 2008; Sømme *et al.*, 2009; Csato *et al.*, 2014; Burgess & Prince, 2015), largely in the context of sequence stratigraphic schemes (Posamentier *et al.*, 1988; Posamentier & Vail, 1988; Van Wagoner *et al.*, 1988; Galloway, 1989; Catuneanu *et al.*, 2009). A prevailing idea/assumption in sequence stratigraphic studies is that a particular segment of the eustatic curve (or accommodation curve) is reflected in a particular sediment stacking pattern (Jervey, 1988; Posamentier & Vail, 1988; Van Wagoner *et al.*, 1988; Galloway, 1989; Embry & Johannessen, 1993), based implicitly or explicitly on the hypothesis of equilibrium response (Muto *et al.*, 2016b). The depositional system growing under base-level cycles is supposed to have no or insignificant hysteresis of the preceding cycles through which the system has been growing.

The recently developed theory of autostratigraphy provides a totally different view from these conventional concepts. It claims that even under steady forcing, the alluvial-shelf system generally cannot sustain a particular style of sediment accumulation but takes non-equilibrium responses (see below) whereby the system autogenically changes its growing pattern through stages. A basic notion in autostratigraphy is that the spatial size of the system at a certain point in time affects how the system evolves thereafter, depending on its own hysteresis (Muto *et al.*, 2016b).

To date, the autostratigraphy theory has been examined mostly in the context of a single distinct rise or fall of the base level (Muto *et al.*, 2016b). To go a step further in autostratigraphic consideration, the present study is devoted to extend it to alluvial-shelf systems growing under steady base-level cycles including rises and falls by means of two-dimensional (2D) physical experimentation. The main research objectives are to clarify: (i) whether and how the autogenic non-equilibrium response changes as the base-level cycles proceed; and (ii) what is the stratigraphic norm of alluvial-shelf systems after experiencing a large number of steady base-level cycles? As documented below, the results of the experiments indicate that an alluvial-shelf system growing through steady base-level cycles of a symmetrical pattern cannot sustain a particular invariable pattern of stratigraphic responses that are manifested in initial/early cycles. The system eventually evolves into a stable phase that with an ever-decreasing aggradation rate is characterized by alternations of non-deltaic transgression during base-level rise and deltaic and aggradational regression during base-level fall.

## LARGE-SCALE AUTOGENESIS UNDER A CONSTANT BASE LEVEL CHANGE

Autogenesis usually refers to 'processes, patterns, or dynamics that arise solely as a consequence of the interaction of the components within a system' (Hajek & Straub, 2017). Two types of autogenesis have been recognized (Hajek & Straub, 2017). One is supposed to be local (small part of the system), cyclic and stochastic, as typically illustrated with channel avulsion and lateral shifting of deltaic lobes (Kim *et al.*, 2014; Li *et al.*, 2016; Paola, 2016). The other type is global (encompassing the entire system), deterministic and non-cyclic. This latter type of autogenesis can account for basin-scale spatial and temporal changes in stratigraphic configuration. Autostratigraphy has been developed to take full consideration of large-scale deterministic autogenesis of depositional systems growing under steady external dynamic forcing (Muto *et al.*, 2007).

Large-scale autogenesis in autostratigraphy commonly takes a form of non-equilibrium response. Non-equilibrium response is a type of response by which steady external forcing results in unsteady stratigraphic configuration and unsteady external forcing can result in steady stratigraphic configuration (Muto *et al.*, 2007, 2016b). As the depositional system grows, it tends to increase in sediment storage capacity, and because of this, fails to sustain a particular fixed configuration. This is the rationale of non-equilibrium responses to steady dynamic

external forcing. Equilibrium response, a type of stratigraphic response by which steady external forcing results in a steady stratigraphic configuration characterized by a particular stratal-stacking pattern, is physically possible (Muto & Swenson, 2006) but does not hold in general (Muto, 2001; Muto *et al.*, 2007; Muto *et al.*, 2014; Muto *et al.*, 2016b).

Recognized large-scale autogenic processes related to a single rise or fall of base level (relative sea level), most of which are manifested as non-equilibrium responses, are summarized in Table 1 and illustrated in Figs 1 and 2. If one assumes the vertical longitudinal profile of a delta as a quadrilateral (Figs 1 and 2), it is notable that even with the same rate of base level change, autogenic non-equilibrium responses experienced by the alluvial-shelf system can vary due to its geometrical conditions (alluvial slope $\alpha$, foreset slope $\beta$, hinterland basement slope $\gamma$ and basin floor slope $\phi$) and pre-existing topographic features (for example, initial alluvial length $L_0$). After the realization of the autoretreat point, for example, continuous base-level rise may eventually reach the moment of autodrowning if the hinterland slope is steeper than the foreset slope (i.e. $\gamma > \beta$; Tomer & Muto, 2010; Table 1; Fig. 1A), or autobreak in the opposite case ($\gamma < \beta$; Muto, 2001; Table 1; Fig. 1 B).

### Autostratigraphic scales

In order to make comparisons between different systems of different scales, the autostratigraphy theory defines length and time scales ($\Lambda$ and $\tau$, respectively; Muto *et al.*, 2007; Muto *et al.*, 2016b). In 2D consideration:

$$\Lambda_{2D} = \frac{q_s}{|R_{bl}|} \quad (1)$$

$$\tau_{2D} = \frac{\Lambda_{2D}^2}{\upsilon} = \alpha \frac{q_s}{|R_{bl}|^2} \quad (2)$$

where $q_s$ is the sediment supply rate per unit width, $R_{bl}$ is the rate of base-level change ($R_{bl} > 0$ for rise; $R_{bl} < 0$ for fall) and $\upsilon$ is the diffusion coefficient for alluvial sedimentation (Paola *et al.*, 1992; Paola, 2000), which can be expressed as $\upsilon = q_S/\alpha$ for linear diffusion (Swenson, 2005). Here the alluvial slope ($\alpha$) is assumed to be a constant value, which might be different from many natural alluvial rivers that tend to decrease in slope in the downstream direction (Kim *et al.*, 2006; Nittrouer *et al.*, 2012; Blom *et al.*, 2016). Considering that, during base-level cycles, the downstream alluvial rivers can tentatively be graded and, when the graded state is attained, are expected to have a uniform and constant slope (Muto & Swenson, 2005, 2006; Swenson & Muto, 2007; Wang *et al.*, 2019b). Thus, it is not unreasonable to assume a particular uniform value for $\alpha$ representing the whole downstream alluvial river.

The term 'large-scale' mentioned above means that the considered length and/or time quantities are much larger than $\Lambda_{2D}$ and $\tau_{2D}$, respectively. $\Lambda_{2D}$ frequently appears in autostratigraphic arguments that are related to characteristic lengths of the depositional system being subject to a base-level change. $\tau_{2D}$, in comparison with a given period of particular forcing, controls how prominently the non-equilibrium response appears for the period. For example, given a period ($T_{bl}$) for a base-level change, the non-equilibrium response is manifested prominently if $\tau_{2D} << T_{bl}$; otherwise, the system may appear to take an equilibrium response if $\tau_{2D} >> T_{bl}$ (Muto & Steel, 1997).

## EXPERIMENTAL DESIGN

The experiments were performed using the experimental facilities at Nagasaki University, including the Margi-6, a stainless steel tank (6.5 m long × 60 cm wide × 1.3 m deep) with a transparent glass wall that allows observation of the entire longitudinal profile of the deltaic shelf system. Inside the tank, a narrow, transparent, parallelogram-shaped acrylic flume (4.1 m long × 2.0 cm wide × 0.57 m deep) was placed (Fig. 3). Sediment and water were supplied at constant rates from the upstream end of the flume to build an alluvial-shelf system. The basement (i.e. the flume floor) was non-erodible and consisted of a downstream 3 m long horizontal part that represented the initial shelf surface (slope $\phi = 0$) and an upstream 1.1 m long, 31° inclined part that served as the hinterland bedrock river (hinterland slope $\gamma = 0.612$ in tangential gradient) (Fig. 3). The flume was open at the downslope end, to keep the water level inside the flume the same as that in Margi-6, playing the role of base level for the experimental alluvial river. The base level was raised and lowered by pumping water to and from Margi-6 using a PC-controlled electromagnetic flowmeter (potential error <1% for base level changing rate).

**Table 1.** Autogenic responses of alluvial-deltaic systems to constant base-level rise and fall.

| Base-level change | Key parameters | Autogenic response | Necessary conditions | References |
|---|---|---|---|---|
| Rise | Initial alluvial length ($L_0$) | Autoretreat (Fig. 1A, B) | | |
| | Critical alluvial length ($L_{crt}$) | Precursory regression | $L_0 < L_{crt}$ ($L_0{}^* < 1$) | Muto (2001) |
| | Hinterland basement slope ($\gamma$) | Deltaic transgression | $T_{bl} >> \tau_{2D}$ ($T_{bl}{}^* >> 1$) | Muto (2001); |
| | Delta foreset slope ($\beta$) | | | Tomer *et al.* (2011) |
| | Period for base-level rise ($T_{bl}$) | Non-deltaic transgression (Fig. 1C, D) | | |
| | | Autodrowning (Fig. 1A, C) | $\gamma > \beta$ | Tomer & Muto (2010) |
| | | | $L = 0$ ($L^* = 0$) | |
| | | Autobreak (Fig. 1B) | $\gamma < \beta$ | Muto (2001) |
| | | | $L = L^{crt}$ ($L^* \sim 1$) | |
| | | Allobreak (Fig. 1C, D) | $L_0 >> L_{crt}$ ($L_0{}^* >> 1$) | Tomer *et al.* (2011) |
| Fall | Delta set thickness ($h_{set}$) | Autogenic grade (Fig. 2C) | $\phi = \alpha$ | Muto & Swenson (2006); |
| | Critical delta set thickness ($h_{set\_crt}$) | | $h_{set} = h_{set\_crt}$ ($h_{set}{}^* = (1+\alpha^{-2})^{-0.5}$) | Muto *et al.* (2016a); |
| | Subaqueous basin floor slope ($\phi$) | | | Wang *et al.* (2019b) |
| | Alluvial slope ($\alpha$) | Autoincision (Fig. 2A) | $\phi > \alpha$ | Muto & Swenson (2005) |
| | Period for base-level fall ($T_{bl}$) | | $h_{set} > h_{set\_crt}$ ($h_{set}{}^* > (1+\alpha^{-2})^{-0.5}$) | |
| | | Sustained aggradation (Fig. 2B) and autogenic detachment | $\phi < \alpha$ | Petter & Muto (2008) |
| | | | $h_{set} < h_{set\_crt}$ ($h_{set}{}^* < (1+\alpha^{-2})^{-0.5}$) | |

Length and time quantities annotated with asterisks indicate the dimensionless forms made by normalizing the real-scale quantity by the autostratigraphic length and time scales (Eqs 1 and 2), respectively.

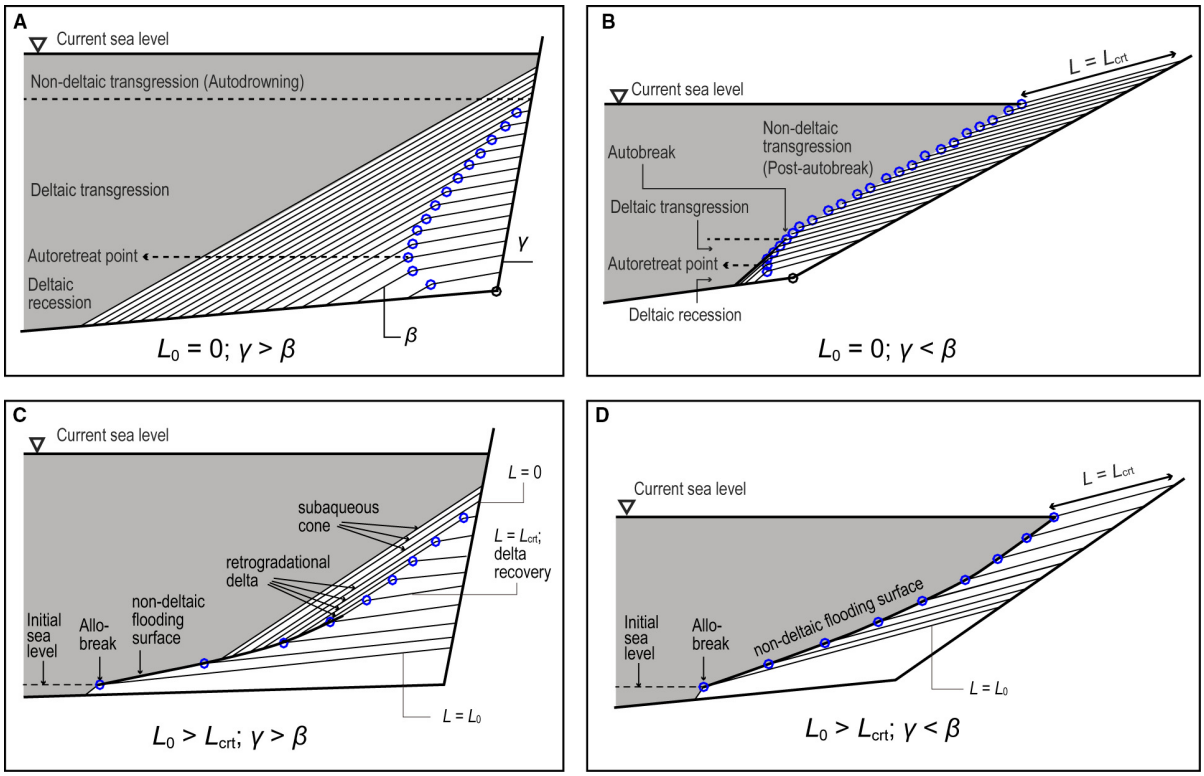


**Fig. 1.** Autogenic non-equilibrium responses of deltas to base-level rise of a constant rate, given a constant rate of sediment supply. (A) Shoreline autoretreat and autodrowning under the slope condition of $\gamma > \beta$. The growing clinoform experiences deltaic recession, deltaic transgression and submerging (autodrowning). After autodrowning, the system becomes non-deltaic although sediment is still supplied by the bedrock river from the hinterland. (B) Shoreline autoretreat and autobreak under the slope condition of $\gamma < \beta$. The growing clinoform experiences deltaic regression, deltaic transgression and non-deltaic transgression. During non-deltaic transgression (after autobreak when deltaic sedimentation is lost), the feeding alluvial river keeps its length at a critical value ($L \sim L_{crt}$). (C) Occurrence of allobreak, non-deltaic transgression, deltaic transgression and autodrowning under the slope condition of $\gamma > \beta$, where the initial alluvial river (or delta) over-extended far beyond $L_{crt}$ prior to the onset of the base-level rise. In this setting, deltaic sedimentation is recovered when the alluvial length has decreased to less than $L_{crt}$. (D) Sustained non-deltaic transgression under the slope condition of $\gamma < \beta$, where the initial alluvial river (or delta) over-extended far beyond $L_{crt}$ prior to the onset of base-level rise. In this setting, deltaic sedimentation during transgression never occurs.

In each experimental run, the base-level cycles had a constant absolute rate of rise and fall ($|R_{bl}|$ = const > 0), a constant period ($T_{bl}$ = const), and thus a constant amplitude ($A_{bl} = |R_{bl}| \times T_{bl}$ = const). All runs started with a base-level rise at the initial basin water depth of 1.0 cm, and the base level was returned to this initial height at the end of every cycle. In total, nine runs with different combinations of $|R_{bl}|$ and $A_{bl}$ were conducted (Fig. 4). Three different values were adopted for $|R_{bl}|$, i.e. low (4.25–4.33 × $10^{-3}$ cm $s^{-1}$), medium (8.54–8.62 × $10^{-3}$ cm $s^{-1}$) and high (12.8–12.9 × $10^{-3}$ cm $s^{-1}$), which means that the lower and higher rates were nearly half and 1.5 times the medium rate, respectively. Three different values were adopted for $A_{bl}$ as well, i.e. low (11.4–11.5 cm), medium (23.1–23.4 cm) and high (46.1–47.9 cm), so that the lower and higher values were half and two times the medium value, respectively. Such a design can help to find out in a systematic way how the rate and amplitude of base-level change affect the construction of alluvial-shelf deposits. Each run was stopped when the downstream or upstream end of the depositional wedge reached the flume edge.

Except for $R_{bl}$ and $A_{bl}$, the same experimental conditions, including sediment material, sediment supply rate and upstream water discharge in unit width ($q_s$ and $q_w$, respectively), were

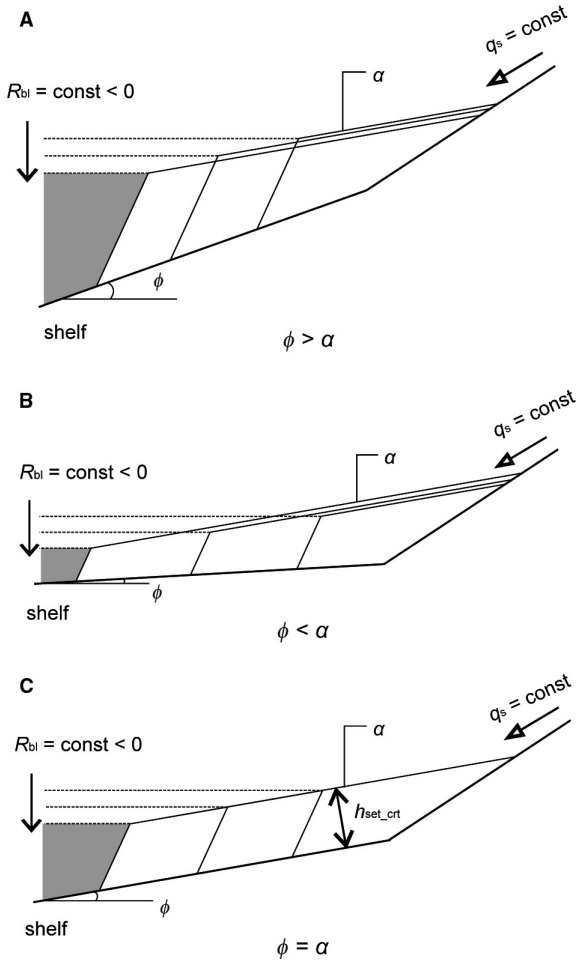


**Fig. 2.** Stratigraphic responses of a river delta to base-level fall of a constant rate ($R_{bl}$ = const < 0), given a constant sediment supply ($q_s$ = const). (A) Degradation (autoincision) of the alluvial river at $\phi > \alpha$ (Muto & Swenson, 2005). (B) Sustained alluvial aggradation at $\phi < \alpha$ (Petter & Muto, 2008). (C) Autogenic attainment of alluvial grade at $\phi = \alpha$, where the longitudinal profile of the deltaic system mimics a parallelogram with a particular set thickness ($h_{set\_crt}$; Muto & Swenson, 2006).

adopted through all runs (Table 2). The sediment used was uniform, natural quartz sand (0.2 mm), to which a small amount of coal powder was added to visualize the internal structure of the deposit. The bulk density of the mixed sediment was 1.38 g cm$^{-3}$. $q_s$ (0.134–0.160 cm$^2$ s$^{-1}$ for all runs, including pore space) and $q_w$ (2.18–2.30 cm$^2$ s$^{-1}$ for all runs) were controlled by a sediment feeder device and a tubing pump, respectively. Owing to the narrowness of the flume, the alluvial sediment-laden flow seldom channelized, avulsed or migrated in the transverse direction, and thus the narrow flume, when viewed from the front side of the tank, represents a 2D longitudinal dip-oriented profile of a marginal depositional wedge. The flow depths were approximately 1 to 2 mm with the Froude number estimated to range between 0.8 and 2.0.

During each run, the positions of three moving boundaries of the depositional wedge, i.e. the delta toe (downlap point), shoreline and the alluvial-basement transition (ABT, onlap point) (Fig. 3), were recorded in digital images (taken every 60 or 30 s). Measurements of the boundary positions in the images are essential for detecting aggradation or degradation of the alluvial-shelf system. For example, downstream migration of the ABT implies degradation or offlap, upstream migration of the ABT implies aggradation or onlap, and the ABT at standstill implies grade (Muto & Swenson, 2005; Kim & Muto, 2007; Muto *et al.*, 2016a).

The conjunction point of the hinterland basement and the initial basin floor of the flume was set as the origin point (0, 0) of an $x$–$z$ coordinate system ($x$, horizontal basinward distance; $z$, vertical upward distance) (Fig. 3). The delta set thickness ($h_{set}$; measured from the shoreline to the delta toe) was measured when it was expanding spatially, mostly during periods of base-level fall. The topset and foreset slopes ($\alpha$ and $\beta$, respectively) were also measured for each run (Table 2), where $\beta$ (0.6–0.7) reflected the angle of repose of the grain-avalanched sediment.

To compare the alluvial-shelf systems built in the nine runs, which were developed in different spatial–temporal frameworks, any designed/measured quantities having units of length $x$ (or $z$) and time $t$ were made dimensionless by dividing them with $\Lambda_{2D}$ and $\tau_{2D}$ (Table 2), respectively. For example, the dimensionless horizontal length $x^* = x/\Lambda_{2D}$, dimensionless vertical height $z^* = z/\Lambda_{2D}$ and dimensionless time $t^* = t/\tau_{2D}$ (the asterisk indicates a dimensionless quantity in this paper). In dimensionless space and time, any discussion of the basin-forcing parameters among experimental runs can be considered scale independent. Table 3 presents a list of dimensionless values. These are the flume size (flume basement length $X_{flume}^*$ and flume depth $Z_{flume}^*$); period for a full base-level cycle ($T_{cycle}^* = 2T_{bl}^*$); amplitude of base-level change ($A_{bl}^*$); critical alluvial length ($L_{crt}^*$), which defines non-deltaic transgression during base-level rise and is given by:

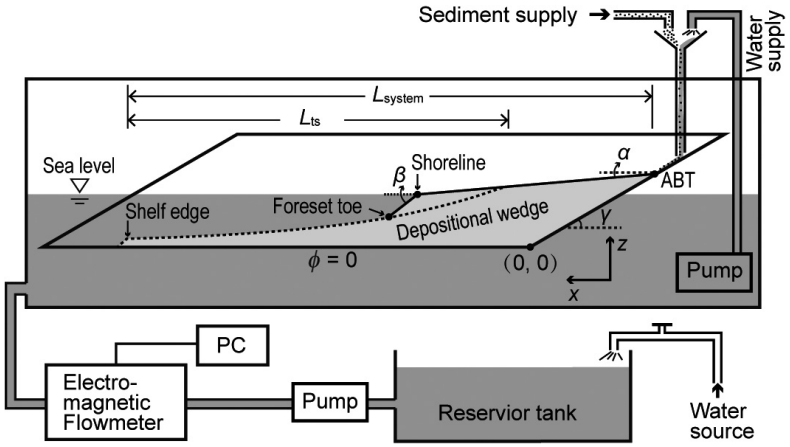


**Fig. 3.** Experimental facilities consisting of a narrow flume placed in a larger, glass-walled observational tank (Margi 6). The built-in flume is so narrow that the flow inside cannot avulse or migrate but only advances forward or retreats backward.

| RunName CyclePeriod ($2T_{bl}$) | | BL oscillation amplitude, $A_{bl}$ (cm) → | | |
|---|---|---|---|---|
| | | Low 11·4–11·5 | Medium 23·1–23·4 | High 46·1–47·9 |
| BL oscillation rate, $\lvert R_{bl}\rvert$ ($10^{-3}$ cm•s$^{-1}$) | Low 4·25–4·33 | LaLr 1·50 h | MaLr 3·00 h | HaLr 6·20 h |
| | Medium 8·54–8·62 | LaMr 0·75 h | MaMr 1·50 h | HaMr 3·00 h |
| | High 12·8–12·9 | LaHr 0·50 h | MaHr 1·00 h | HaHr 2·00 h |

**Fig. 4.** Matrix of experimental design of the nine runs which were yielded by three values of $A_{bl}$ and three values of $|R_{bl}|$. In each cell are the run names on the top and periods for base-level cycles ($2T_{bl}$, for a rise and a subsequent fall) on the bottom.

$$L_{crt} = \frac{\gamma\sqrt{1+\alpha^2}}{\gamma-\alpha}\Lambda_{2D} \tag{3a}$$

$$L^*_{crt} = \frac{L_{crt}}{\Lambda_{2D}} = \frac{\gamma\sqrt{1+\alpha^2}}{\gamma-\alpha} \tag{3b}$$

and critical delta set thickness ($h_{set\_crt}$*), which distinguishes aggradation and degradation during base-level fall and is given by:

$$h_{set\_crt} = \frac{\Lambda_{2D}}{\sqrt{1+\alpha^{-2}}} \tag{4a}$$

$$h^*_{set\_crt} = \frac{h_{set\_crt}}{\Lambda_{2D}} = \frac{1}{\sqrt{1+\alpha^{-2}}}. \tag{4b}$$

Among the parameters listed in Table 3, $A_{bl}$* is also key to the present study, as will be shown later; it is given by:

$$A^*_{bl} = \frac{A_{bl}}{\Lambda_{2D}} = \frac{R^2_{bl}T_{bl}}{q_s} \tag{5a}$$

By combining Eq. 2 based on the assumption of linear diffusion, Eq. 5a is equivalent to Eq. 5b:

$$A^*_{bl} = \alpha\frac{T_{bl}}{\tau_{2D}} = \alpha T^*_{bl} = \frac{\alpha}{2}T^*_{cycle} \tag{5b}$$

Similar to many other geometric models, the 2D experiment presented below does not incorporate complex physical processes including morphodynamics and tectonics, but simplifies the stratigraphic problems into geometric questions. With the geometry of sediment surfaces and basin configurations, stratigraphic stacking patterns can be predetermined (Paola, 2000).

## EXPERIMENTAL RESULTS

### Reference run: medium amplitude and medium rate

#### *Conditions adopted*

The medium amplitude and medium rate (MaMr) run was conducted with a medium amplitude and medium rate of base-level change (Fig. 4), serving as a representative example for outlining all experimental results. With $|R_{bl}| = 8.62 \times 10^{-3}$ cm s$^{-1}$ and $q_s = 0.147$ cm$^2$ s$^{-1}$, $\Lambda_{2D}$ was calculated as 17.0 cm (Eq. 1). With a

**Table 2.** Experimental parameters.

| Run name | Upstream sediment supply rate in unit width: $q_s$ ($cm^2\ s^{-1}$) | Upstream water discharge in unit width: $q_w$ ($cm^2\ s^{-1}$) | Rate of base-level change: $\lvert R_{bl}\rvert$ ($cm\ s^{-1}$) | Period for base-level cycle: $T_{cycle}$ (= $2T_{bl}$) (h) | Amplitude of base-level cycle: $A_{bl}$ (cm) | Total run time: $t$ (h) | Average alluvial slope: $\alpha$ | Average foreset slope: $\beta$ | 2D autostratigraphic length scale: $\Lambda_{2D}$ (cm) | 2D autostratigraphic time scale: $\tau_{2D}$ (s) | Critical alluvial length during base-level rise: $L_{crt}$ (cm) | Critical delta set thickness during base-level fall: $h_{set\_crt}$ (cm) |
|---|---|---|---|---|---|---|---|---|---|---|---|---|
| LaLr | 0.140 | 2.291 | 0.00425 | 1.50 | 11.5 | 12.00 | 0.139 | 0.697 | 32.9 | 1077.1 | 43.00 | 4.53 |
| MaLr | 0.145 | 2.344 | 0.00433 | 3.00 | 23.4 | 17.57 | 0.139 | 0.653 | 33.4 | 1068.3 | 43.60 | 4.59 |
| HaLr | 0.142 | 2.300 | 0.00430 | 6.20 | 47.9 | 18.45 | 0.145 | 0.625 | 33.1 | 1119.1 | 43.85 | 4.76 |
| LaMr | 0.159 | 2.290 | 0.00862 | 0.75 | 11.4 | 12.90 | 0.135 | 0.620 | 18.4 | 289.2 | 23.85 | 2.47 |
| MaMr | 0.147 | 2.285 | 0.00862 | 1.50 | 23.3 | 13.50 | 0.143 | 0.658 | 17.0 | 281.6 | 22.40 | 2.40 |
| HaMr | 0.134 | 2.177 | 0.00854 | 3.00 | 46.1 | 15.00 | 0.158 | 0.608 | 15.7 | 291.5 | 21.45 | 2.46 |
| LaHr | 0.155 | 2.227 | 0.0128 | 0.50 | 11.5 | 12.48 | 0.134 | 0.647 | 12.1 | 126.8 | 15.65 | 1.61 |
| MaHr | 0.160 | 2.215 | 0.0128 | 1.00 | 23.1 | 14.00 | 0.148 | 0.605 | 12.5 | 143.4 | 16.65 | 1.82 |
| HaHr | 0.158 | 2.250 | 0.0129 | 2.00 | 46.5 | 15.00 | 0.158 | 0.600 | 12.3 | 149.6 | 16.77 | 1.91 |

**Table 3.** Dimensionless experimental parameters.

| Run name | Dimensionless length of the flume basement $X_{flume}$* | Dimensionless depth of the flume basement $Z_{flume}$* | Dimensionless period for a full base-level cycle $T_{cycle}$* (= $2T_{bl}$*) | Dimensionless amplitude of the base-level cycle $A_{bl}$* | Dimensionless critical alluvial length during base-level rise $L_{crt}$* | Dimensionless critical set thickness during base-level fall $h_{set\_crt}$* |
|---|---|---|---|---|---|---|
| LaLr | 9.12 | 1.72 | 5.01 | 0.35 | 1.31 | 0.138 |
| MaLr | 8.98 | 1.70 | 10.11 | 0.70 | 1.31 | 0.137 |
| HaLr | 9.06 | 1.71 | 19.94 | 1.45 | 1.32 | 0.144 |
| LaMr | 16.30 | 3.08 | 9.34 | 0.62 | 1.30 | 0.134 |
| MaMr | 17.65 | 3.34 | 19.18 | 1.37 | 1.32 | 0.141 |
| HaMr | 19.11 | 3.61 | 37.05 | 2.94 | 1.37 | 0.156 |
| LaHr | 24.79 | 4.69 | 14.20 | 0.95 | 1.29 | 0.133 |
| MaHr | 24.00 | 4.54 | 25.10 | 1.85 | 1.33 | 0.146 |
| HaHr | 24.39 | 4.61 | 48.13 | 3.78 | 1.36 | 0.156 |

measured value of $\alpha$ (= 0.143 on average), $\tau_{2D}$ was estimated as 281.6 s (Eq. 2). $\Lambda_{2D}$ and $\alpha$ yielded a value of 22.4 cm for $L_{crt}$ (critical alluvial length during base-level rise, Eq. 3a) and 2.40 cm for $h_{set\_crt}$ (critical set thickness during base-level fall; Eq. 4a). In this run, nine base-level cycles were performed with $A_{bl}$* = 1.37, $T_{bl}$* = 9.59, $L_{crt}$* = 1.32 and $h_{set\_crt}$* = 0.141 (Tables 2 and 3).

*Results*

Stratigraphical responses of the alluvial-shelf system to the base-level rise varied significantly through cycles, as shown in Fig. 5A to I, where each image was taken at the end of the base-level rise. During the base-level rise in cycle 1 (Fig. 5A), the alluvial-shelf system first experienced deltaic regression ($t^*$ = 0–0.85, $t$ = 0–240 s), then deltaic transgression ($t^*$ = 0.85–5.5, $t$ = 240–1560 s) and finally non-deltaic transgression ($t^* \geq 5.5$, $t \geq 1560$ s) when the alluvial length was nearly constant ($L^*$ = 1.22 ~ $L_{crt}$*). From cycle 2 onward, non-deltaic transgression occurred as soon as the rise began. The resulting flooding surface in each cycle steepened upstream to develop a concave-upward geometry, that is, the local basin slope just basinward of the shoreline ($\phi_{local}$) progressively increased landward (Fig. 5B and C). As the cycles proceeded, the flooding surface, as a whole, became gentler and less curved and its average slope ($\phi_{avg}$, shelf edge to shoreline) decreased to approach the alluvial slope ($\alpha$) (Fig. 5D to I): $\phi_{avg} \sim \alpha$ at the end of base-level rise in cycles 8 and 9.

The stratigraphical response of the alluvial-shelf system to the base-level fall significantly changed through cycles as well, as shown in Fig. 5J to R which were taken at the end of each base-level fall. In cycle 1, the delta prograded initially onto the subaqueous depositional surface and then onto the horizontal basement surface, accompanied by net downstream migration of ABT (Fig. 5J). This subaerial degradation was also recognized in subsequent cycles 2 and 3, although to less significant extents than the subaerial degradation in cycle 1 (Fig. 5K and L). A fundamental difference in cycles 2 and 3 from cycle 1 is that for most of the regression time (i.e. base-level fall), a delta prograded onto a distinctively concave-upward surface that was generated by non-deltaic flooding during the preceding base-level rise. In cycles 4 and later, the ABT was subjected to net upstream migration (Fig. 5M to R), and no clear signals of degradation were found. As the flooding surface progressively became gentler as the cycles proceeded, the local basin floor in front of the delta became almost linear and the delta set became thinner.

Figure 6 shows the trajectories of the ABT, shoreline and delta toe in $x^*$–$t^*$ space, the initial and final river lengths at the onset and end of each base-level rise ($L_0$* and $L_{final}$*, respectively), and $h_{set}$* during each base-level fall (note that $h_{set}$* makes sense only for base-level

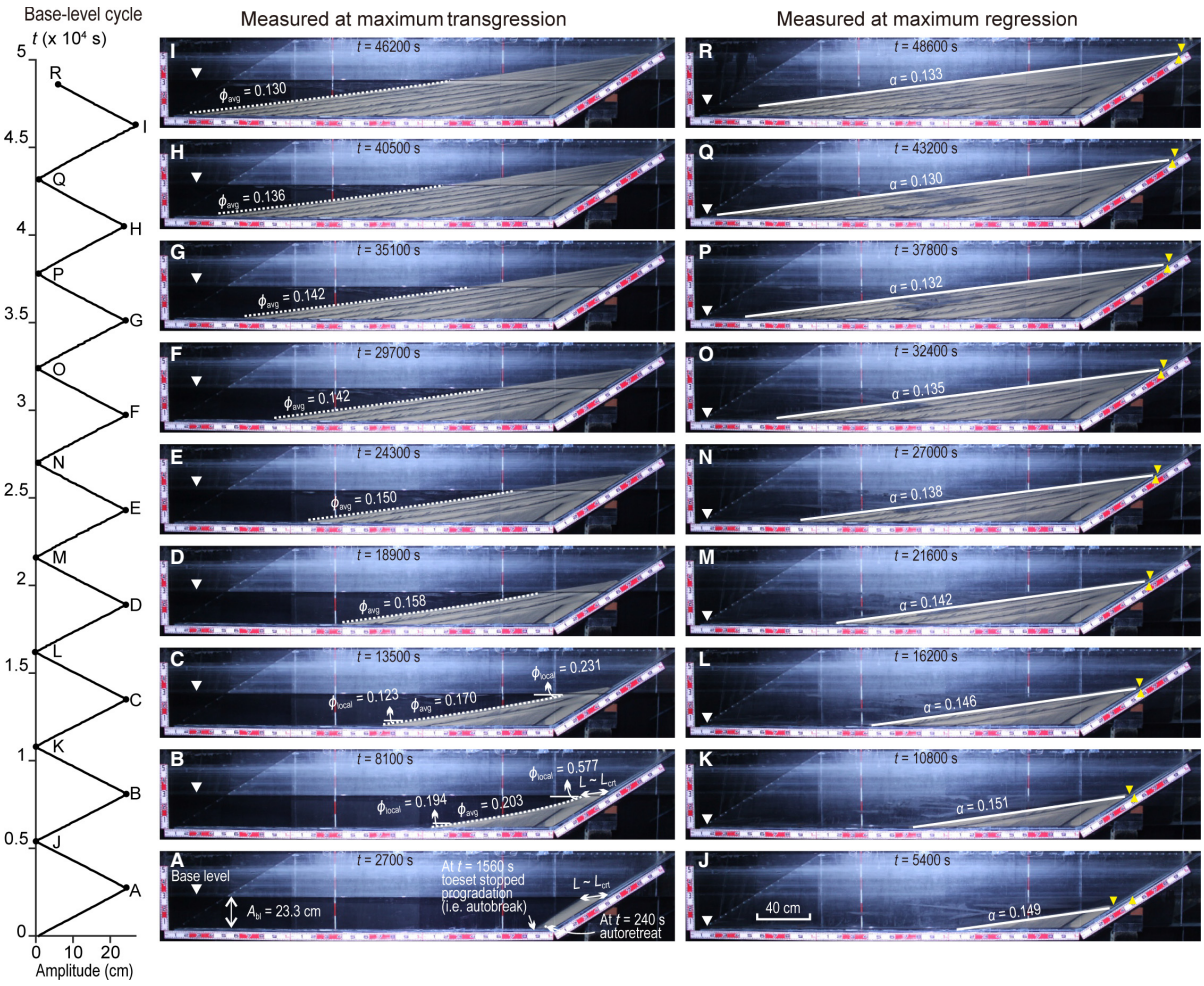


**Fig. 5.** Sequential photographic images of the alluvial-shelf system built in the reference run MaMr (medium amplitude and medium rate), taken right after periods of base-level rise (A) to (I) and fall (J) to (R), along with the base-level scenario. Dotted white lines in (A) to (I) highlight maximum flooding surface in the cycle. Solid lines in (J) to (R) highlight alluvial surfaces at maximum regression in the cycle. White inverted triangle indicates current base level. Paired yellow triangles indicate positions of the onlap point or the alluvial-basement transition (ABT): inverted yellow triangle indicates the current one (at maximum regression), while upright yellow triangle indicates ABT position at the previous maximum transgression. Note that as base-level cycles proceeded: (i) the alluvial river at maximum regression became longer; (ii) the maximum flooding surface became longer and flatter; and (iii) in late cycles the maximum flooding surface almost coincided with the alluvial profile that was built during the preceding base-level fall.

fall); all are in phase with the base-level changes. In Fig. 6B (for cycles 1 to 3, see the close-up shot), the shoreline trajectory of the cycle 1 base-level rise was initially directed basinward ($t^* < 0.85$); then it retreated landward in a curved pattern and then in a linear pattern, the latter of which happened after the delta toe became inactive (at $t^* \sim 5.5$). During the base-level rise in cycles 2 and 3, the shoreline trajectory exhibited a curved transgressive profile. During the base-level rise in cycles 4 and later, the shoreline trajectory was almost linear, documenting that the flooding surfaces became flatter, i.e. the same pattern as shown in Fig. 5B to I.

For the base-level falling limbs, the following phenomena are notable (Fig. 6B and D). (i) In cycles 1 to 3, the ABT migrated downstream after a short period of upstream migration. This upstream to downstream transition of the ABT

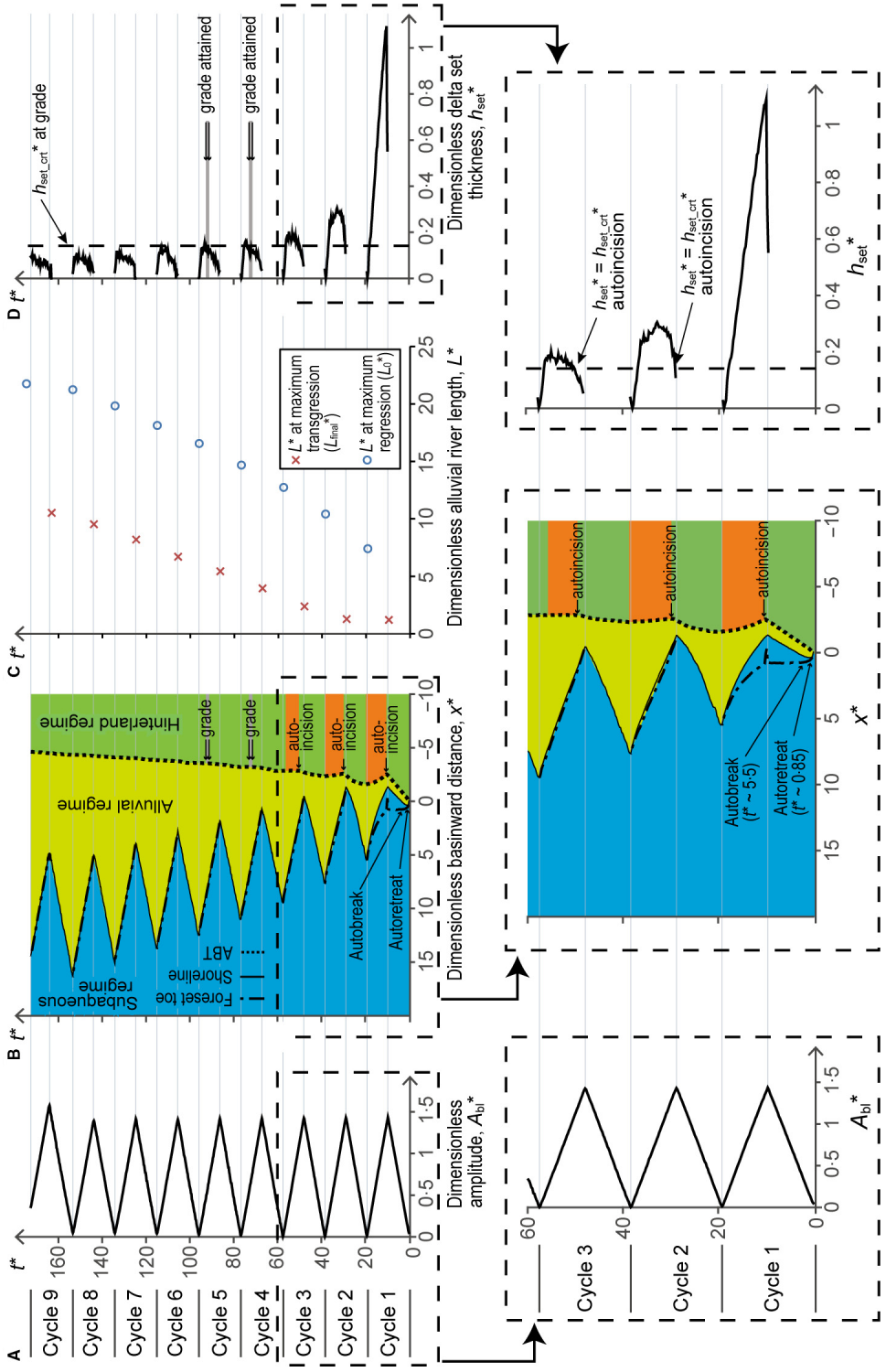


**Fig. 6.** Time correlations of data from reference run MAMR (medium amplitude and medium rate). (A) Base-level oscillations. (B) Onlap and downlap pinchouts in $x^*$–$t^*$ space. (C) Dimensionless initial and final river lengths before and after each base-level rise ($L_0^*$ and $L_{final}^*$). (D) Time correlations of $h_{set}^*$ during base-level fall. The vertical dotted line indicates $h_{set\_crt}^*$. Note that: (i) in cycles 1 to 3, base-level rise gave rise to a steeper and curved shoreline trajectory, and in response to base-level fall, autoincision did not occur until when $h_{set}^* > h_{set\_crt}^*$; (ii) autogenic grade of the feeder alluvial river was attained during the falling limb in cycles 4 and 5, as indicated with the stabilized ABT (the onlap point) and the equality of $h_{set}^*$ with $h_{set\_crt}^*$; and (iii) in cycles 6 to 9, shoreline trajectories for base-level rise limbs were closely linear, and $h_{set}^* < h_{set\_crt}^*$ during the falling limbs indicating sustained aggradation. Light orange hatch indicates time intervals for degradation, otherwise degradational-free. Dark grey hatch indicates the time interval for the attainment of grade. Thin grey horizontal lines refer to time lines at the end of base-level rise and fall.

occurred when the delta set thickness ($h_{set}$) tentatively became close to the theoretical critical value ($h_{set\_crt}$). From cycles 1 to 3, the condition of $h_{set} \sim h_{set\_crt}$ was realized for a successively longer time after the onset of each base-level fall (see the close-up shot for autoincision in Fig. 6B and D). The $h_{set}$ values then significantly exceeded $h_{set\_crt}$ to reach a maximum value ($h_{set\_max}$), after which $h_{set}$ decreased. (ii) From cycle 4 onward, the ABT no longer migrated downstream, while $h_{set\_max}$ progressively decreased and finally became smaller than $h_{set\_crt}$. (iii) Specifically, $h_{set}$ (or $h_{set\_max}$) in cycles 4 and 5 reached and sustained the magnitude of $h_{set\_crt}$ ($h_{set}^* \sim h_{set\_crt}^*$), during which the ABT remained stationary.

The growing processes of deltaic shelves through base-level cycles can be outlined by the variations in several measured parameters (Table 4), including the successive increase in $L_0$ (as well as $L_{final}$) and successive decreases in $h_{agg\_blr}$ (aggradational thickness during base-level rise), $\phi_{avg}$ and $h_{set\_max}$. Table 4, along with Figs 5 and 6, documents that: (i) through cycles of base-level rise and fall, the alluvial-shelf system as a whole experienced net elongation (progradation) and net aggradation, although both progressively decreased in rate; (ii) the flooding surface became gentler and less curved; and (iii) transgressive–regressive units became thinner.

*Interpretation*

*During base-level rise*. The non-equilibrium response of the alluvial-shelf system to the base-level rise changed as the base-level cycles proceeded. The first cycle showed the full process from shoreline autoretreat (regression to transgression) to autobreak (deltaic to non-deltaic environments), owing to the sufficiently long period of base-level rise ($T_{bl} \sim 10\tau_{2D}$) (Muto, 2001). From cycle 2 onward, the alluvial-shelf system was subjected to non-deltaic transgression without being preceded by deltaic regression and deltaic transgression, reflecting over-extension of the alluvial river ($L_0 = 125.9$ cm $> L_{crt}$, at the beginning of cycle 2) and thus an allobreak event (Tomer *et al.*, 2011).

During the non-deltaic (especially post-allobreak; Tomer *et al.*, 2011) transgression recognized in cycles 2 to 9, the entire supplied sediment was consumed only for building the alluvial reaches. Therefore, the aggradation rate ($R_{agg}$) and length ($L$) of the alluvial river are in a reciprocal relationship:

**Table 4.** Measurements of length and slope parameters in the reference run MAMR (medium amplitude and medium rate).

| Base-level change | Key parameters | Cycle 1 | Cycle 2 | Cycle 3 | Cycle 4 | Cycle 5 | Cycle 6 | Cycle 7 | Cycle 8 | Cycle 9 |
|---|---|---|---|---|---|---|---|---|---|---|
| Rise | Alluvial length before rise: $L_0$ (cm) | 0.0 | 125.9 | 177.2 | 216.6 | 249.6 | 281.7 | 308.4 | 337.4 | 361.2 |
| | Alluvial length after rise: $L_{final}$ (cm) | 20.6 | 21.7 | 40.6 | 67.3 | 92.6 | 113.9 | 139.5 | 162.3 | 179.0 |
| | Aggradation thickness by rise: $h_{agg\_blr}$ (cm) | 20.0 | 7.16 | 3.09 | 2.08 | 2.00 | 1.54 | 1.45 | 1.17 | 1.36 |
| | Average shelf slope after rise: $\phi_{avg}$ | 0.678 | 0.203 | 0.170 | 0.158 | 0.150 | 0.142 | 0.142 | 0.135 | 0.130 |
| Fall | Maximum set thickness by fall: $h_{set\_max}$ (cm) | 16.3 | 4.56 | 3.0 | 2.21 | 2.21 | 2.05 | 1.70 | 1.58 | 1.56 |

$$q_s \sim LR_{agg} \left(q_s = \text{const} > 0\right) \quad (6)$$

Thus, $R_{agg}$ tends to increase as the over-extended alluvial river shortens (but is still longer than $L_{crt}$). Equation 6 explains the continual changes in the flooding surface geometry. In a single event of base-level rise, the flooding surface tended to steepen landward, reflecting the decrease in alluvial length ($L$), whereby the flooding surface as a whole developed a concave-upward geometry. As the cycles proceeded, the entire flooding surface became gentler and less curved, gradually approaching the pre-existing alluvial profile ($\phi_{avg} \sim \alpha$) and corresponding to an overall increase in alluvial length ($L$), because the increase in $L_0$ was always greater than the increase in $L_{final}$ (Table 4; Fig. 6C).

*During base-level fall.* In Fig. 6B, the degradational, aggradational and graded stages of the feeder alluvial river can be distinguished from the behaviour of the ABT and the measured values of $h_{set}$* relative to $h_{set\_crt}$*.

The ABT's basinward turnabout, which took place in each of the first three cycles, documents autoincision (Muto & Steel, 2004; Swenson & Muto, 2007). Autoincision was reached after an initial aggradation phase, which became longer through cycles 1 to 3 (Fig. 6B). This successively longer delay in the attainment of autoincision is due to the average shelf slope becoming gentler through cycles (but still $\phi_{avg} > \alpha$). After reaching a maximum value, $h_{set}$ decreased, reflecting the basinward decrease in shelf slope (i.e. $\phi$) (Fig. 5B and C). The degradation sustained in cycles 1 to 3 after the realization of autoincision is due to the set thickness of the prograding delta always being larger than the theoretical value ($h_{set} > h_{set\_max}$). It should be noted that at the end of each base-level fall, $h_{set}$ suddenly increased and then decreased. This occurred when the delta toe prograded beyond the existing shelf edge and then onto the horizontal basement ($\phi = 0$).

The stationary ABT, along with the set thickness ($h_{set}$*) values being equal or very close to the critical value ($h_{set\_crt}$*) observed in cycles 4 and 5, suggests that the basinward-extending alluvial river attained autogenic grade. This was realized because of: (i) the delta prograding onto the sufficiently long, subaqueous surface having a slope ($\phi_{avg}$) equal/close to the alluvial slope ($\alpha$); and (ii) the period of base-level fall ($T_{bl}$), which was sufficiently long to allow the alluvial-shelf system to adjust its set thickness to reach the critical value ($h_{set} \sim h_{set\_crt}$).

In cycles 6 to 9, the alluvial river feeding the delta aggraded during the entire periods of base-level fall, as documented by the ABT steadily migrating upstream and all $h_{set}$* values being lower than the $h_{set\_crt}$* value. The progressive decrease in delta set thickness through cycles was due to the progressive extension of the alluvial-shelf system, whereby the delta was able to prograde steadily over a longer distance with a lower aggradation rate. As an inevitable result, the period of base-level fall ($T_{bl}$ = const) became increasingly insufficient to realize $h_{set} \sim h_{set\_crt}$.

## Comparative runs

For the comparative eight runs, Figs 7 to 10 show the base-level scenarios adopted, the resultant trajectories of the three moving boundaries (i.e. ABT, shoreline, and delta toe) in $x$*–$t$* space, the initial and final alluvial lengths ($L_0$* and $L_{final}$*, respectively) for each base-level rise, and temporal changes in delta set thickness values ($h_{set}$*) during each base-level fall. The runs are described here in groups of three runs, which include the reference run (MaMr).

### *Group 1 with variations in amplitude: HaMr–MaMr–LaMr*

*Conditions.* This run group includes the high-amplitude medium-rate run HaMr, the medium-amplitude medium-rate reference run MaMr and the low-amplitude medium-rate run LaMr. This group served as a reference for modulations of the base-level changing amplitude ($A_{bl}$) (Fig. 4). The runs were conducted with similar $|R_{bl}|$ conditions that yielded $\Lambda_{2D}$ and $\tau_{2D}$ values being nearly the same between runs (Table 2). The HaMr and LaMr runs were performed with amplitudes (and periods) of base-level changes that were doubled and halved from those in the reference MaMr run, respectively (Tables 2 and 3).

*Results.* The HaMr run realized five cycles (Fig. 7A), during which the alluvial-shelf system evolved into a pattern similar to that in earlier cycles of the reference run (MaMr). In the first base-level rise, landward retreat of shoreline occurred at $t$* = 0.82 ($t$ = 240 s). Subsequently, until $t$* ~ 5.6 ($t$ ~ 1620 s), the system started to evolve as a non-deltaic alluvial river, when the alluvial river reached a length ($L$* = 1.35,

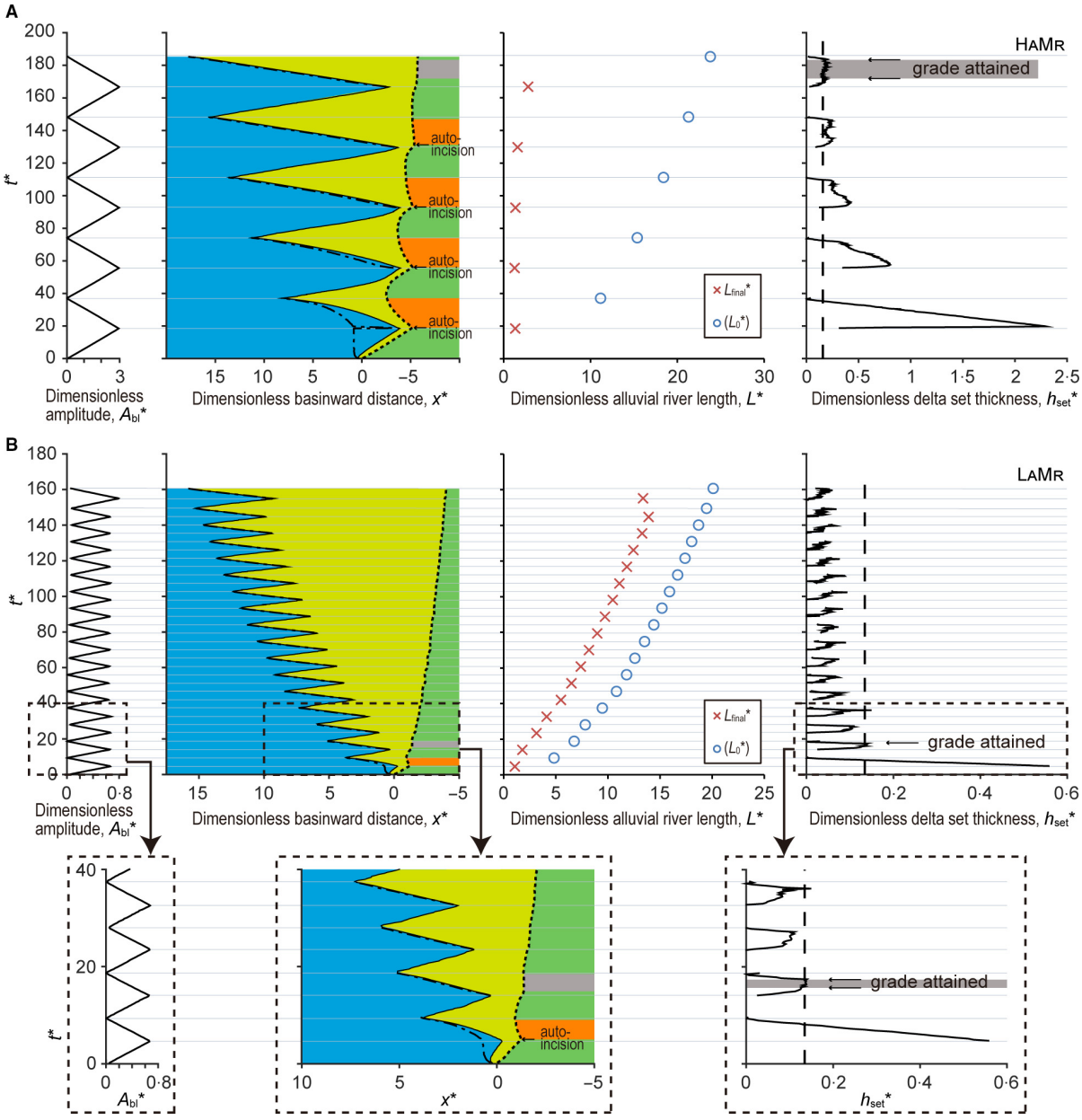


**Fig. 7.** Time correlations of data measured in comparable runs. (A) The high-amplitude medium-rate run HAMR. (B) The low-amplitude medium-rate run LAMR. Legends as in Fig. 6. Note that the *x*-axis scales are different in (A) and (B).

$L$ = 21.2 cm) close to the theoretical value ($L_{crt}$ = 21.4 cm). During the following base-level rises, transgression caused a significant inundation, leaving the maximum flooding surface in a significantly curved profile (see the curved shoreline trajectory particularly in cycles 2 and 3). During base-level falls, the ABT migrated downstream and the delta set thickness reached a value significantly exceeding the critical value ($h_{set\_crt}$ = 2.46 cm). In subsequent cycles, the maximum flooding surface of each cycle was gradually flattened, the downstream transition of the ABT became less prominent, and $h_{set\_max}$ tended to decrease. Until cycle 5, $\phi_{avg} \sim \alpha$, the

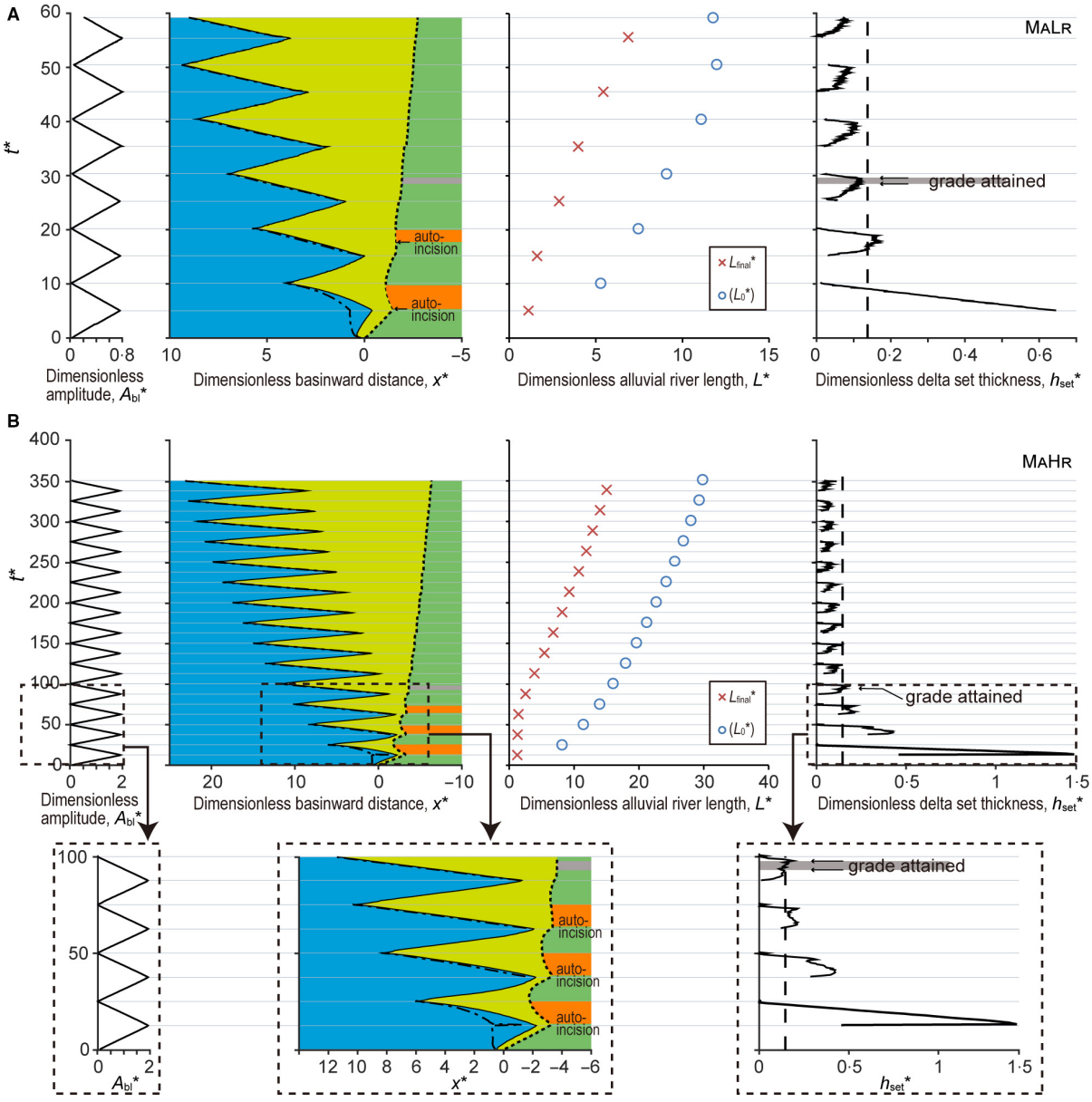


**Fig. 8.** Time correlations of data measured in comparable runs. (A) The medium-amplitude low-rate run MALR. (B) The medium-amplitude high-rate run MAHR. Legends as in Fig. 6. Note that the *x*-axis scales are different in (A) and (B).

ABT was stabilized, and $h_{set} \sim h_{set\_crt}$. These phenomena occurred during much later cycles in the higher-amplitude run (HAMR), compared to their occurrence in the reference run.

The LAMR run realized 17 cycles (Fig. 7B). In the first base-level rise, the shoreline started to retreat landward at $t^* = 1.0$ ($t = 300$ s). Different from the other two runs, the alluvial-shelf system in this low-amplitude run maintained deltaic sedimentation during the entire first base-level rise. Meanwhile, the alluvial river kept increasing in length to reach a value of 19.6 cm ($L^* = 1.07$, $L = 19.6$ cm), which was less than the estimated $L_{crt}$ value (23.8 cm), i.e. non-deltaic transgression was not realized. From cycle 2 onward, the alluvial-shelf system

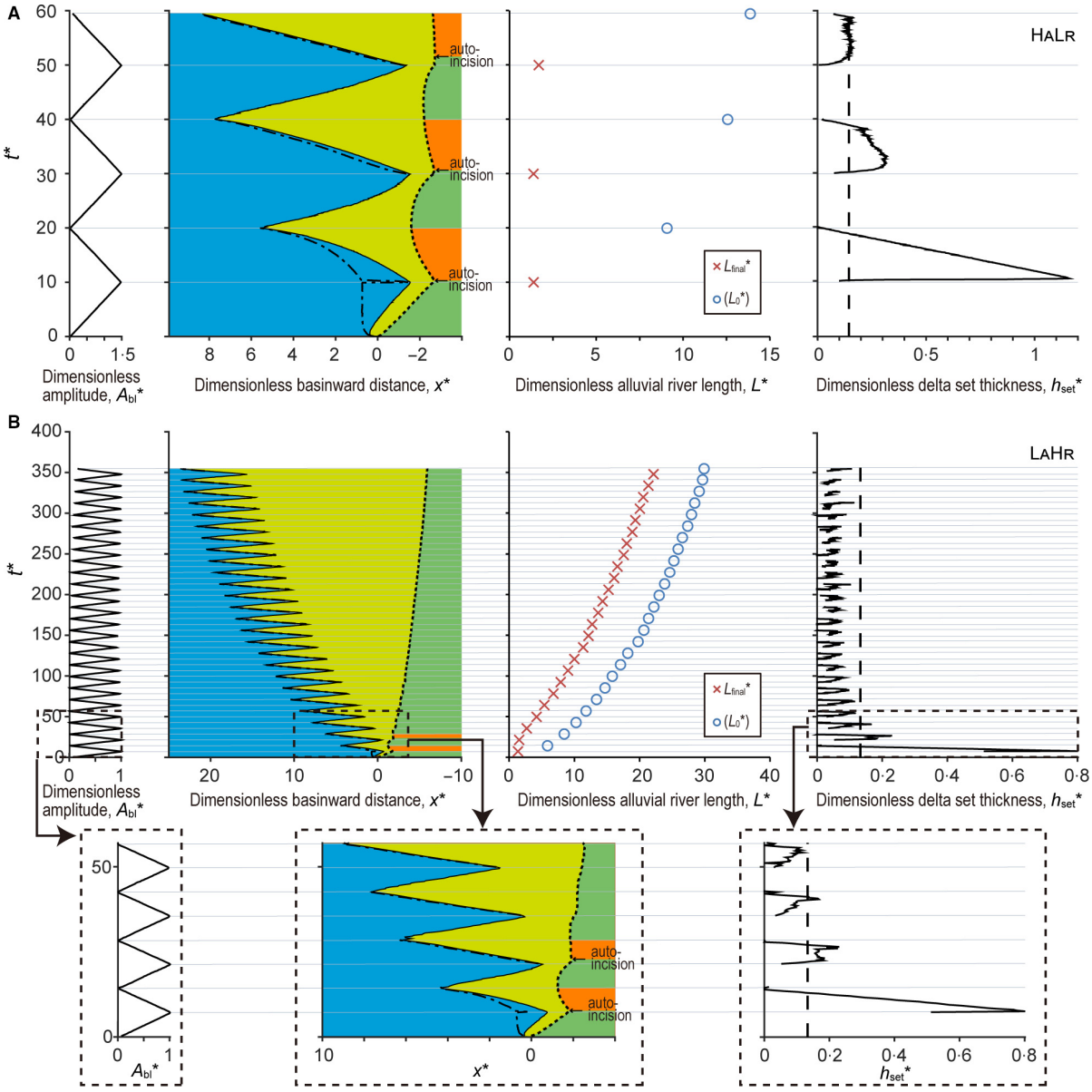


**Fig. 9.** Time correlations of data measured in comparable runs. (A) The high-amplitude low-rate run HALR. (B) The low-amplitude high-rate run LAHR. Legends as in Fig. 6. Note that the *x*-axis scales are different in (A) and (B).

evolved into a pattern analogous to what occurred in later cycles of the reference MAMR run, that is: (i) during periods of base-level rise, transgression inundated only a smaller portion of the existing depositional wedge and the flooding surface was nearly flat; and (ii) during periods of base-level fall, the delta extended basinward without downstream transition of the ABT, and the delta set thickness kept increasing during the progradation but was always smaller than $h_{set\_crt}$. Specifically, during cycle 2, the relationship $h_{set} \sim h_{set\_crt}$ and the stabilization of ABT were attained much earlier than those attained in runs with high and medium amplitudes (i.e. HAMR and MAMR).

*Interpretation*. Because the amplitude (or period) of base-level change is the only variable among the three runs (Table 2), the different amplitudes account for the observed differences

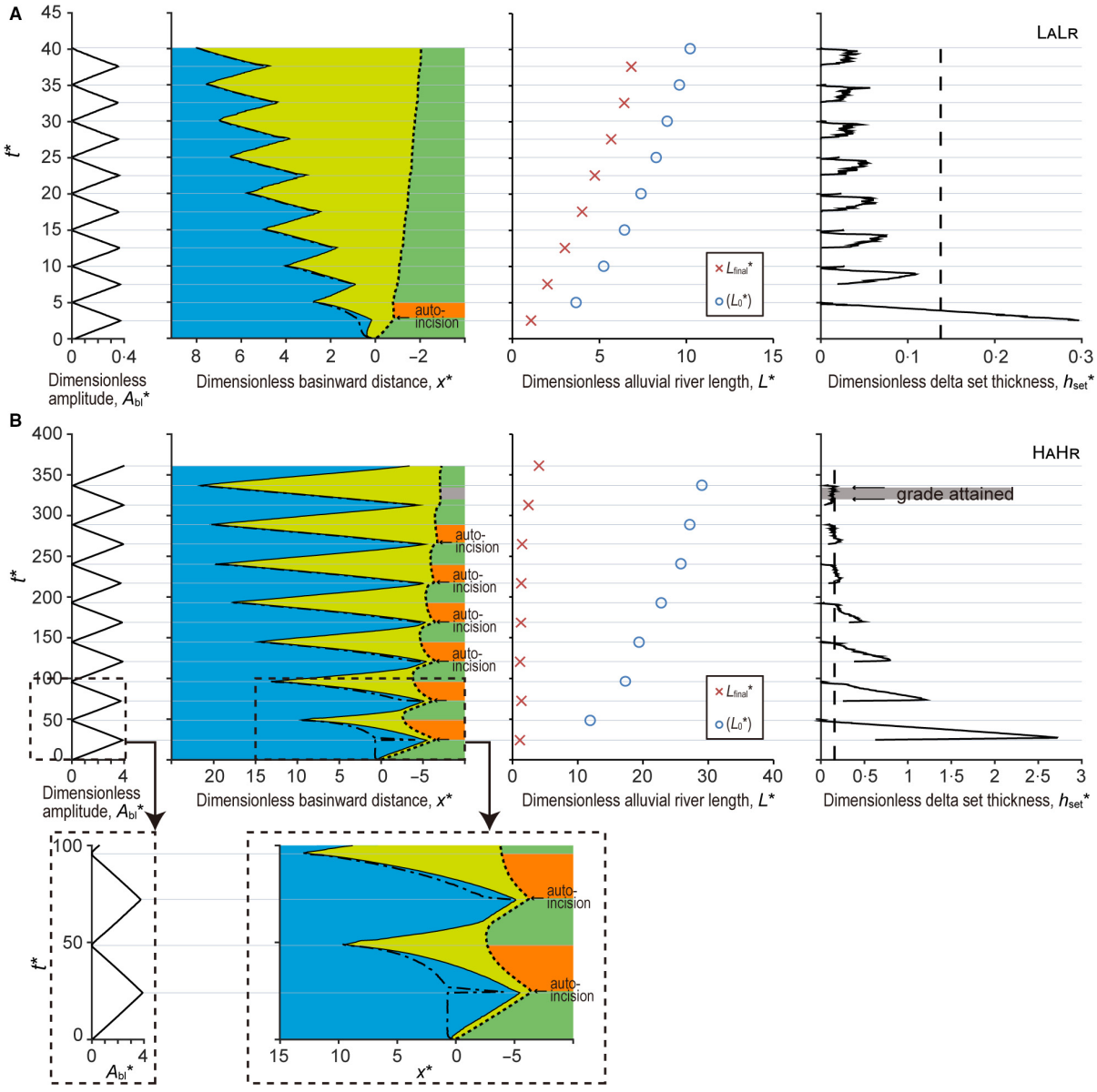


**Fig. 10.** Time correlations of data measured in comparable runs. (A) The low-amplitude low-rate run LALR. (B) The high-amplitude high-rate run HAHR. Legends as in Fig. 6. Note that the *x*-axis scales are different in (A) and (B).

in stratigraphy. In the first rise of the HAMR run, the duration of base-level rise ($T_{bl}$) was long enough to manifest both autoretreat and autobreak. In the succeeding cycles, the base-level rise always caused non-deltaic transgression because of the over-extension of the alluvial river. Owing to the higher amplitude, the base-level rise was more capable of shortening the alluvial reaches. According to Eq. 6, the flooding surfaces were generally steeper ($\phi_{avg} >> \alpha$ at maximum flooding) than those produced in contemporary cycles in the reference run (MAMR). With the steeper shelf (i.e. large $\phi_{avg}$), in turn, the base level falling more easily forced the delta to grow with a delta set thickness larger than the critical value. Therefore, the alluvial-shelf system more quickly attaining autoincision and degradation was pervasive during base-level fall. In other words, a higher amplitude has a greater impact on the modification of the

alluvial-shelf system. As a consequence, more cycles were required to create a gentler shelf ($\phi_{avg} \sim \alpha$) with which autogenic grade was realized, as compared to the reference run (MaMr).

In the LaMr run, the low amplitude had a low impact on deforming the alluvial-shelf system. For the first cycle, the base-level rise was sufficient to manifest autoretreat, but insufficient for autobreak to occur. Non-deltaic transgression started from cycle 2. Owing to the reduced amplitude, transgression was less capable of shortening the alluvial reaches, and thus the flooding surface was less curved than that of the reference run (Eq. 6). Therefore, the slope condition of $\phi_{avg} \sim \alpha$ was achieved earlier, and autogenic grade was reached earlier as well. Following this grade cycle, degradation never occurred because the slope condition of $\phi_{avg} \sim \alpha$ was sustained during the rest of the base-level falls. The alluvial-shelf system sustained an aggradational regime during the rest of the periods of base-level rise and fall because $T_{bl}$ became insufficient to realize alluvial grade after the second grade cycle.

*Group 2 with variations in rate: MaLr–MaMr–MaHr*

*Conditions.* This run group includes the medium-amplitude low-rate run MaLr, the medium-amplitude medium-rate reference run MaMr and the medium-amplitude high-rate run MaHr. This group with the same intermediate amplitude ($A_{bl}$) served as a reference for modulations of base-level change rate ($|R_{bl}|$) (Fig. 4). Runs with lower and higher rates (i.e. $|R_{bl}|$) of base-level change were performed 0.5 times and 1.5 times as fast as the MaMr run, respectively. Therefore, the alluvial-shelf systems of this group were controlled by different values of $\Lambda_{2D}$ and $\tau_{2D}$: for the low-rate run (MaLr), $\Lambda_{2D}$ = 33.4 cm and $\tau_{2D}$ = 1068.3 s (the $\Lambda_{2D}$ and $\tau_{2D}$ were approximately twice and four-times as high as the values of the reference MaMr run), while for the high-rate run (MaHr), $\Lambda_{2D}$ = 12.5 cm and $\tau_{2D}$ = 143.4 s (the $\Lambda_{2D}$ and $\tau_{2D}$ were approximately 2/3 and 4/9 of the values of the reference MaMr run) (Table 2). Normalized with larger and smaller $\Lambda_{2D}$ (or $\tau_{2D}$), $A_{bl}$ and $T_{bl}$ were scaled down in the low-rate run (MaLr) and scaled up in the high-rate run (MaHr), respectively (for example, $A_{bl}^*$ = 0.70 for MaLr and 1.85 for MaHr, see Table 3).

*Results.* Despite the different $\Lambda_{2D}$ and $\tau_{2D}$ values, the alluvial-shelf growth patterns documented in these three runs bear significant similarities to one another (Fig. 8). First, in earlier cycles, the base-level rise created more curved flooding surfaces, and the base-level fall led to the downstream transition of the ABT and higher values of delta set thickness (for example, $h_{set\_max}$). Second, as the cycles proceeded, the entire flooding surface became gentler and flatter, $h_{set\_max}$ became smaller, and the ABT never migrated downstream irrespective of whether the base level was falling or rising. Third, there existed a base-level cycle during which the ABT was stabilized and the condition $h_{set}^* \sim h_{set\_crt}^*$ was maintained.

The results of this run group also show significant differences. In the low-rate run (MaLr), the alluvial-shelf system was subjected to six cycles (i.e. 2/3 of the reference MaMr run) (Fig. 8A). In the first cycle, the shoreline landward retreat was manifested at $t$ = 780 s (i.e. more than double the time at which autoretreat was manifested in the reference MaMr run). In dimensionless timescales, they were almost equivalent ($t^*$ = 0.73 for the MaLr run, $t^*$ = 0.85 for the MaMr run) (Figs 6 and 8A). On the other hand, non-deltaic transgression was not attained during the first base-level rise, and the critical alluvial length ($L_{crt}^*$) was not reached (Fig. 8A). Stabilization of the ABT and the condition $h_{set}^* \sim h_{set\_crt}^*$ were realized during the base-level fall of cycle 3 ($t^*$ = 28.3–29.5), earlier than those in the reference MaMr run. Before this critical cycle, the landward inundation during base-level rise, the downstream transition of the ABT, and the discrepancy between $h_{set\_max}^*$ and $h_{set\_crt}^*$ (during base-level falls) were less distinct compared to those of the reference MaMr run.

In the MaHr run, the alluvial-shelf system was subjected to 14 base-level cycles, reflecting smaller length and time scales than that in the reference MaMr run (Fig. 8B). For the base-level rise in cycle 1, both events of landward retreat of shoreline ($t^*$ = 0.84, $t$ = 120 s) and non-deltaic transgression ($t^*$ = 4.18, $t$ = 600 s) were manifested. In the real scale, these occurred earlier than those in the reference MaMr run (in which autoretreat and autobreak occurred at $t$ = 240 s and 1560 s, respectively). Again, in dimensionless scales, the three runs were almost equivalent, i.e. the autoretreat point occurred at $t^*$ = 0.73–0.85 and autobreak occurred at $t^*$ = 4.2–5.5 (Figs 6 and 8B). During cycle 4, stabilization of the ABT and the condition $h_{set}^* \sim h_{set\_crt}^*$ were realized during $t^*$ = 94.0–98.3, a

bit later than in the reference MaMr run ($t^*$ = 74.1). Meanwhile, before the critical cycle, the landward inundation during base-level rise, the downstream transition of the ABT, and the discrepancy between $h_{set\_max}^*$ and $h_{set\_crt}^*$ (during base-level falls) were much greater in the MaHr run than in the other two runs.

*Interpretation.* In these three runs, the base-level changes were at different rates while the amplitude remained constant. The different $R_{bl}$ values imply that the alluvial-shelf systems grew with different intrinsic scales ($\Lambda_{2D}$ and $\tau_{2D}$ in Eqs 1 and 2). Comparing these three runs makes sense only when the dimensionless length and time quantities (for example, $A_{bl}^*$ and $T_{bl}^*$) are considered. For example, in the real time space, the moment of shoreline autoretreat took place later and earlier in runs with lower and higher rates, respectively. In the dimensionless time space, the autoretreat point was reached at almost the same time.

In the MaLr run, the dimensionless amplitude and period of the base-level cycle were reduced with larger length and time scales ($A_{bl}^*$ = 0.70, $T_{bl}^*$ = 5.06) than in the reference run (MaMr, where $A_{bl}^*$ = 1.37 and $T_{bl}^*$ = 9.59; Table 3), whereby the effect of base-level change on the alluvial-shelf system was less. In the first cycle, for example, the amplitude of base-level rise was sufficient to realize shoreline autoretreat but insufficient to realize an autobreak event. In addition, because of the reduced $T_{bl}^*$ and $A_{bl}^*$ values, the base-level rise was less capable of shortening the alluvial reaches, and the produced shelf was much gentler than that created during contemporary cycles in the reference run (MaMr). Consequently, the degradation during base-level fall tended to be less prominent. Because a shelf slope approximately equal to the alluvial slope ($\phi_{avg} \sim \alpha$) was realized after a smaller number of cycles, autogenic grade was attained in earlier cycles than it was in the reference run.

In the MaHr run, the dimensionless amplitude and period of the base-level cycle were amplified ($A_{bl}^*$ = 1.85, $T_{bl}^*$ = 12.55). In the first cycle, the base-level rise was sufficient to manifest both autoretreat and autobreak. In addition, the base-level rise was more capable of shortening the alluvial reaches, which resulted in steeper shelves. Consequently: (i) the slope condition of $\phi_{avg} \sim \alpha$ was realized later, the attainment of autogenic grade was delayed; and (ii) degradation during the cycles preceding the graded cycle/stage was more prominent.

*Group 3 with opposite variations in amplitude and rate: HaLr–MaMr–LaHr*

*Conditions.* The high-amplitude low-rate (HaLr) and low-amplitude high-rate (LaHr) runs were also performed with $|R_{bl}|$ values that were *ca* 0.5 times and *ca* 1.5 times higher than that in the reference run (MaMr), respectively. As a result, the $\Lambda_{2D}$ value for the HaLr and LaHr runs was approximately twice and two-thirds as high as that for the MaMr run, respectively; and the $\tau_{2D}$ value was approximately four-times and 4/9 as compared to that in the MaMr run, respectively (Table 2). Meanwhile, the base-level amplitudes ($A_{bl}$) adopted for the HaLr and LaHr runs were approximately doubled and halved, respectively, as compared to those in the MaMr run, i.e. a higher value of $A_{bl}$ was adopted for the larger $\Lambda_{2D}$ run. After normalization with $\Lambda_{2D}$ (or $\tau_{2D}$), the $A_{bl}^*$ (and $T_{bl}^*$) values for the three runs were similar (for example, $A_{bl}^*$ = 1.45 for the HaLr run, 1.37 for the MaMr run, and 0.95 for the LaHr run). Thus, this group represents alluvial-shelf growing styles under various $\Lambda_{2D}$ but with similar $A_{bl}^*$ ($T_{bl}^*$ as well; Table 3).

*Results.* In the HaLr run, only three cycles were completed (Fig. 9A), where the shoreline trajectory for each base-level rise tended to be curved ($\phi > \alpha$), and the ABT during base-level fall tended to migrate downstream accompanied by the inequality $h_{set}^* > h_{set\_crt}^*$. In the base-level rise of cycle 1, both events of landward retreat of shoreline ($t^*$ = 0.70) and non-deltaic transgression ($t^*$ = 5.42) were manifested at nearly the same $t^*$ values as in the reference MaMr run. No grade was attained through all cycles, as documented by the ABT migrating downstream even in the last cycle of base-level fall.

In the LaHr run, 25 cycles were performed (Fig. 9B). Similar to HaLr, both events of landward retreat of shoreline and non-deltaic transgression were manifested in the first base-level rise (at $t^*$ = 0.71 and 4.97, respectively). From cycle 3 onward, the alluvial-shelf system evolved into an aggradational phase, similar to that in the reference MaMr run, during which landward inundation was less significant, the maximum flooding surface was nearly flat, the ABT never migrated downstream irrespective of the continuing base-level changes, and the delta set thickness ($h_{set}^*$) was always smaller than the critical value ($h_{set\_crt}^*$).

The growing pattern of the alluvial-shelf systems produced by these three runs shared similarities (Figs 6 and 9). The three-cycle HaLr run

 

is analogous with the first three cycles of the other two runs. The nine-cycle reference run (MaMr) is closely equivalent to the first nine cycles of the LaHr run. The 25-cycle LaHr run simply represents the continuous evolution of the alluvial-shelf system for a longer spectrum of $t^*$ with a higher number of cycles.

*Interpretation.* As interpreted for group 2, alluvial-shelf systems growing with larger intrinsic scales (for example, the HaLr run) are less sensitive to base-level changes. In these group runs, a higher amplitude of the base level is adopted for runs with larger intrinsic scales and when the dimensionless amplitude ($A_{bl}^*$) and period of base-level changes ($T_{bl}^*$) are close. Therefore, the base-level change had a similar impact on the growth of the system in these three runs.

During cycle 1, the base-level rise was sufficient to cause both autoretreat and autobreak. In the succeeding cycles, because the $A_{bl}^*$ (or $T_{bl}^*$) values were similar for the three runs, the extent of the shortening of alluvial rivers and the curved profiles of non-deltaic transgressive surfaces with base-level rise were similar in the runs, and the base-level fall allowed the alluvial-shelf system to extend basinward to a similar extent as well (in dimensionless space). This means that in the dimensionless space–time framework, these three runs are nearly equivalent. As a consequence, the alluvial-shelf system evolved from the degradation-inclusive phase into the aggradation-sustainable phase at a comparative time ($t^*$).

### *Group 4 with in-phase variations in amplitude and rate: LaLr–MaMr–HaHr*

*Conditions.* The low-amplitude low-rate (LaLr) run and high-amplitude high-rate (HaHr) run were conducted with the rates of base-level change ($|R_{bl}|$) being *ca* 0.5 times and *ca* 1.5 times as fast as that in the reference MaMr run, respectively. Thus, the $\Lambda_{2D}$ value for the former and latter was also approximately twice and two-thirds as high as that in the reference run (MaMr), respectively; and the $\tau_{2D}$ value was also approximately four-times and 4/9 as high as that in the MaMr run, respectively (Table 2). Meanwhile, the amplitudes of base-level change ($A_{bl}$) adopted for runs with lower-amplitude (LaLr) and higher-amplitude (HaHr) were approximately half and twice, respectively, as high as that adopted in the MaMr run, i.e. a higher value of $A_{bl}$ was adopted for the smaller $\Lambda_{2D}$ run. Contrary to group 3, the normalized $A_{bl}^*$ values for the LaLr and HaHr runs were further reduced and amplified as compared to the values for the MaMr run (for example, $A_{bl}^* = 0.35$ for the LaLr run, 1.37 for the MaMr run, and 3.78 for the HaHr run). The three runs of this group thus represent alluvial-shelf growing styles under extremely low, medium and extremely high values of $A_{bl}^*$ ($T_{bl}^*$ as well; Table 3); the LaLr and HaHr are 'end-member' runs in terms of $A_{bl}^*$ (and $T_{bl}^*$) values among the nine runs.

*Results.* In the LaLr run, eight cycles were performed (Fig. 10A). During the first cycle, the base-level rise caused a landward retreat of shoreline at $t^* = 0.84$, close to that in the reference MaMr run. Non-deltaic transgression was not realized. From cycle 2 onward, the system grew in a pattern that resembled the aggradation-sustainable phase of the reference MaMr run in that the following occurred: (i) during the base-level rise, the transgression inundated a smaller part of the entire system and the shoreline trajectory exhibited a linear pattern reflecting the flatness of the flooding surface; and (ii) during each base-level fall, the ABT kept migrating upstream, and the delta set thickness, which was always smaller than the critical value ($h_{set}^* < h_{set\_crt}^*$ always), kept decreasing.

The HaHr run comprised seven cycles (Fig. 10B), during most of which the alluvial-shelf system grew with a similar pattern to that during the earlier cycles in the reference MaMr run. In the base-level rise of cycle 1, both events of landward retreat of shoreline (which occurred at $t^* = 0.80$) and non-deltaic transgression (which occurred at $t^* = 5.21$) were manifested at nearly the same $t^*$ values in the reference MaMr run. In the rest of the cycles, during base-level rise, the transgression resulted in flooding of a large part of the alluvial realm, which left steeper flooding surfaces ($\phi_{avg} > \alpha$); during base-level fall, the ABT migrated downstream and the delta set thickness reached a value that significantly exceeded the critical value. Compared with phenomena observed in the reference MaMr run, the base-level rise caused inundation to a greater landward extent, and the base-level fall resulted in a longer downstream transition of the ABT and a larger delta set thickness. In addition, the grade cycle (cycle 7) was realized much later.

*Interpretation.* The dimensionless amplitude ($A_{bl}^*$) and period ($T_{bl}^*$) of the base-level change

again account for the differences among the three runs. The values of $A_{bl}$* and $T_{bl}$* in the LaLr run were the lowest among the values of the nine runs. Thus, the base-level cycle had the least effect on the evolution of the alluvial-shelf system. For example, in the first base-level rise, the amplitude was sufficient to realize shoreline autoretreat but insufficient to realize an autobreak event; thus, non-deltaic transgression was not realized. In the succeeding cycles, the base-level rise caused least landward inundation and the alluvial river was not shortened as much as in the other runs. The shelves were least curved and most flattened, with which the base-level fall caused least degradation. As a result, the shelf slope became gentler and approached the alluvial slope ($\phi_{avg} \sim \alpha$) just after the first cycle, and the system evolved into an aggradation-sustainable phase almost immediately. Autogenic grade was not attained during any base-level falls because the period of base-level fall and/or the length of shelf were very limited to let the delta grow until reaching a thickness value close to the theoretical value (i.e. $h_{set}$* was always smaller than $h_{set\_crt}$*; Fig. 10).

The $A_{bl}$* and $T_{bl}$* values in the HaHr run were the highest, whereby the base-level changes had the greatest impact during the growth of the alluvial-shelf system. In the first cycle, the base-level rise caused both autoretreat and autobreak. During the succeeding cycles, the base-level rise caused more prominent inundation and was more effective in shortening the river and creating steeper shelves, by which autoincision was easily realized and degradation was intense during the base-level fall. It was not until the later cycles that the system grew to a size that was sufficient to resist the influence of base-level changes. In the latest cycles, the shelf surface became sufficiently gentler ($\phi_{avg} \sim \alpha$) and autogenic grade was attained eventually.

### Flooding surfaces produced by base-level rise

In all nine runs, the configuration of the flooding surface varied as the base-level cycles proceeded. The first base-level rise in every run created a subaqueous depositional slope. In runs with low $A_{bl}$* values (LaMr, MaLr and LaLr), autobreak of deltaic sedimentation was not attained, and thus the entire subaqueous slope was of delta foreset with a gradient of $\beta$. In the runs where autobreak was attained (MaMr, HaMr, HaLr, HaHr, MaHr and LaHr), the subaqueous slope was characterized by $\beta$ for the lower part (before autobreak) and by $\gamma$ for the upper part (after autobreak; parallel to the hinterland slope). It is not clear in the experiment because of the closeness between $\beta$ and $\gamma$. Starting from cycle 2, the flooding surfaces were starved of sediment and steepened landward. The steepness of the flooding surfaces was reduced as the cycles proceeded. Clearly, the influence of the base-level cycles decreased, as the entire system expanded.

Four characteristic parameters were used to analyse the evolution of the configuration of maximum flooding surfaces, namely the dimensionless horizontal length of the entire depositional system ($L_{system}$*) (Fig. 3), the dimensionless horizontal length of the maximum flooding surfaces ($L_{ts}$*) (Fig. 3), the transgressive ratio ($I_{ts}$) given by $L_{ts}$*/$L_{system}$* and the average shelf slope ($\phi_{avg}$). Figure 11 illustrates how $L_{system}$*, $L_{ts}$*, $I_{ts}$ and $\phi_{avg}$ varied with the base-level cycles in each run, showing that as the base-level cycles proceeded; (i) $L_{system}$* gradually increased; (ii) $L_{ts}$* increased but showed a tendency to approach a constant value; (iii) $I_{ts}$ decreased; and (iv) $\phi_{avg}$ gradually decreased to approach a constant value equal to the alluvial slope (i.e. $\alpha$).

These experimental results can be explained as follows. (i) With steady base-level cycles of a symmetrical pattern and constant sediment supply, the entire alluvial-shelf system tended to expand, particularly with basinward extension. (ii) As a consequence, the maximum flooding (at the end of base-level rise) overlaid a smaller portion of the entire system ($I_{ts}$ decreasing). (iii) As the base-level cycles proceeded further, the flooding surface became flatter and approached a gradient of the alluvial river ($\alpha$), and thus $L_{ts}$* progressively increased to approach a constant length specified by $A_{bl}$*$\alpha^{-1}$. From Fig. 11 one can interpret that runs with a higher $A_{bl}$* show more significant inundation (larger $L_{ts}$* and larger $I_{ts}$), supporting the aforementioned interpretations.

## DISCUSSION

### Effects of growth of the alluvial-shelf system

The experimental results suggest that the spatial growth of the alluvial-shelf system does not allow its particular stratigraphic responses in the initial/early stages to be sustained through steady base-level cycles of a symmetrical

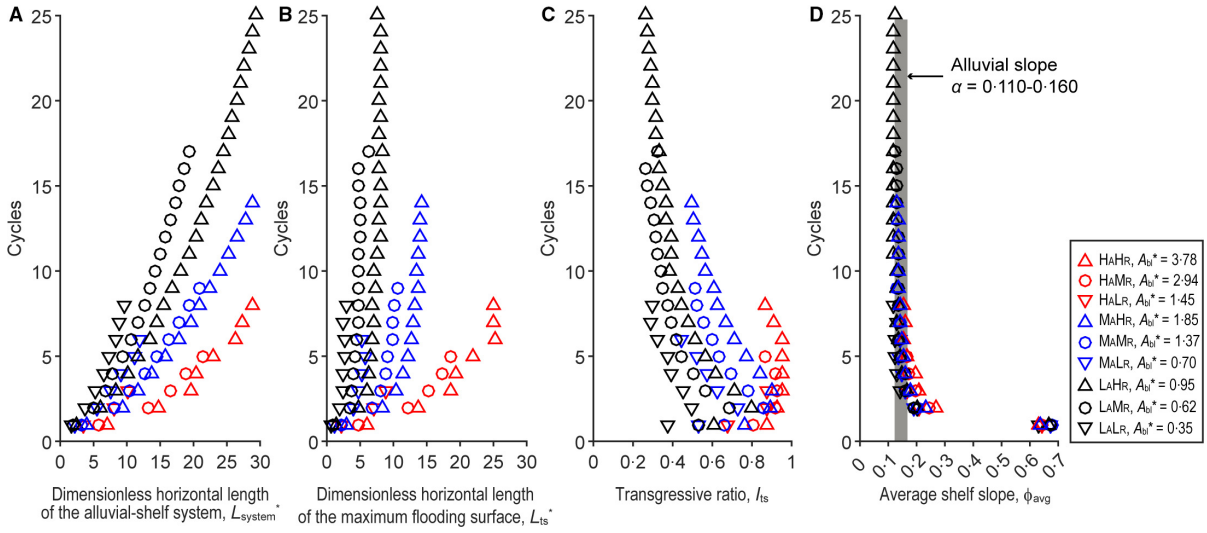


**Fig. 11.** Cycle-lapsed data measured from experimental runs, related to maximum flooding in each cycle. (A) Dimensionless horizontal length of the whole depositional system ($L_{system}$*) (Fig. 3). (B) Dimensionless horizontal length of the maximum flooding surface ($L_{ts}$*) (Fig. 3). (C) Transgressive ratio ($I_{ts}$) set by $L_{ts}$*/$L_{system}$*. (D) Averaged flooding surface slope ($\phi_{avg}$) measured from the shelf edge to the shoreline. Note that as base-level cycles proceeded, the gradient of the flooding surface closely approached that of the alluvial river (i.e. $\alpha$) at the end of the preceding base-level fall.

pattern. A consequence of repeated base-level changes is that at the onset of each base-level rise (except for the first cycle), there is a pre-existing deposit characterized by an alluvial river profile that has extended basinward during the preceding base-level fall. After a larger number of base-level cycles have proceeded, the pre-existing deposit will have a larger volume of accumulated sediment and a longer alluvial profile. Because of this, progressive growth of the alluvial-shelf system, the aggradation rate of the entire system tends to decrease with the base-level cycles. As a result: (i) the average shelf slope created during base-level rise tends to be gentler (Eq. 6); and (ii) the set thickness of the delta prograding during base-level fall tends to decrease and, after a number of base-level cycles, can be much smaller than $h_{set\_crt}$. This latter concept suggests that a shelf-transiting alluvial system will eventually become free from degradation and retain an aggradational regime as long as the base-level cycles continue.

The deterministic changes, in general, may include the following scenario. During earlier cycles, the base-level rise creates a curved flooding surface ($\phi_{avg} > \alpha$). As a consequence, the subsequent base-level fall causes degradation. In a mid-cycle, when the system has sufficiently extended basinward ($L^* >> 1$), transgression with the base-level rise realizes the slope condition of $\phi_{avg} \sim \alpha$, and autogenic grade is attained during the subsequent base-level fall (for example, groups 1 and 2) (Muto & Swenson, 2006). After this grade phase, continuing base-level cycles further make the alluvial-shelf system extend basinward ($L^*$ increases). Although the slope condition of $\phi_{avg} \sim \alpha$ can be sustained during transgressions of the following cycles, autogenic grade is no longer realized because the response time of the prograding delta to reach the critical set thickness ($h_{set\_crt}$) exceeds the period for the base-level fall ($T_{bl}$) (Nijhuis *et al.*, 2015). As a result, the shelf system starts an aggradation-sustainable phase.

To summarize, distinct non-equilibrium responses in the initial/early cycles, such as shoreline autoretreat and autobreak with base-level rise and autoincision with base-level fall, tend not to occur in later cycles, and instead converge to monotonous equilibrium responses that are characterized by non-deltaic transgression during base-level rise and by deltaic and aggradational regression during base-level fall (Fig. 12). During this transition from the early degradation-inclusive cycles to the late aggradation-sustainable cycles, there can be transient cycle(s) when the alluvial river attains autogenic grade with base-level fall. Such an unsteady but

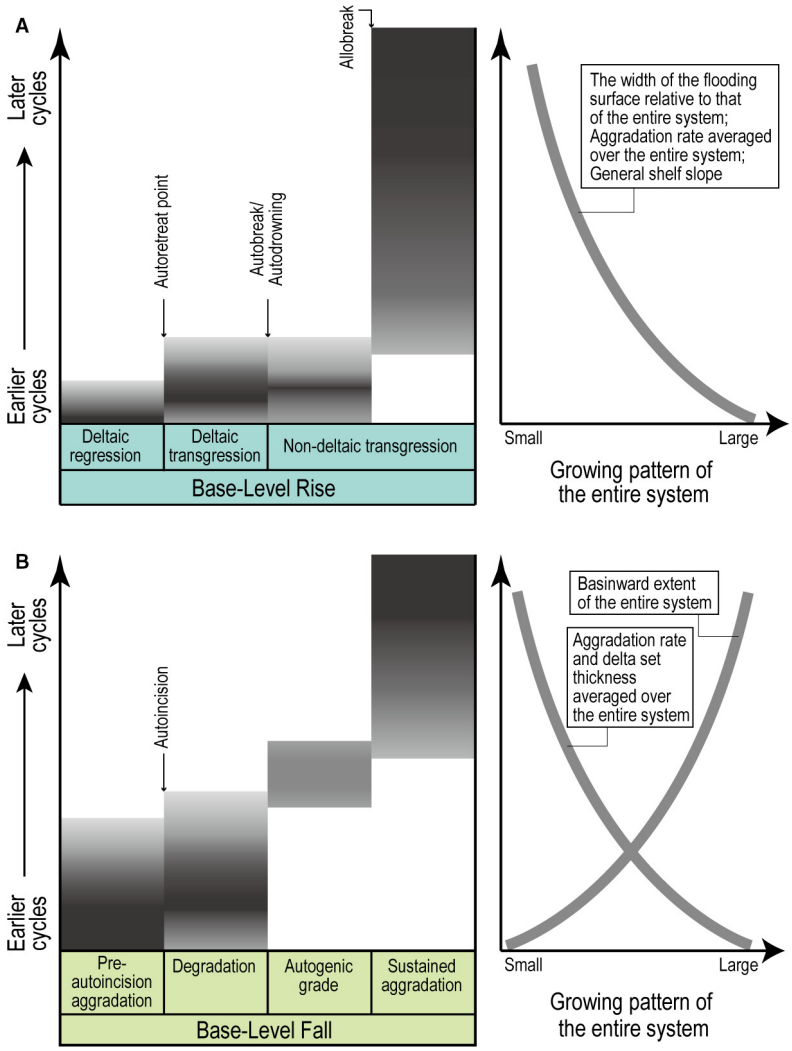


**Fig. 12.** Phase diagram showing changes of primary stratigraphic responses of shelf-transiting alluvial systems in response to steady base-level cycles of a symmetrical pattern. The darkness of the colour band indicates the likelihood of the corresponding stratigraphic response. (A) Stratigraphic responses during rising limbs. (B) Stratigraphic responses during falling limbs.

deterministic growth pattern of the system may be regarded as an 'overall' autogenic non-equilibrium response to 'overall' steady dynamic external forcing. Such an evolution pattern can also be interpreted in terms of the spatial expansion of the alluvial-shelf system and thus the progressive reduction of the effect of the base-level changes upon the system.

## The effect of base level amplitude and changing rate

The deterministic changes in the autogenic non-equilibrium response can differ in detail owing to the base-level conditions ($A_{bl}$, $T_{bl}$ and $|R_{bl}|$), which are embodied in the dimensionless base-level changing amplitude (i.e. $A_{bl}$*, Eqs 5a and 5b). According to the experiment, larger $A_{bl}$* tends to be more effective in shortening the alluvial part and producing a steeper flooding surface and thus might delay the shelf system from entering the aggradation-sustainable phase. The number ($N_{bl}$) of base-level cycles that is required before the shelf system enters the aggradation-sustainable phase can be roughly expressed as (Fig. 13):

$$N_{bl} \sim 2A^*_{bl} \quad (7)$$

This relation is rather empirical and independent of the geometrical model. It is based largely on mass balance and does not include the influence of grain-size variation. Its significance is to document that alluvial-shelf systems growing with a higher $A_{bl}$* need to have a larger $L$* to attain the slope condition of $\phi \sim \alpha$, which is required for the attainment of autogenic grade,

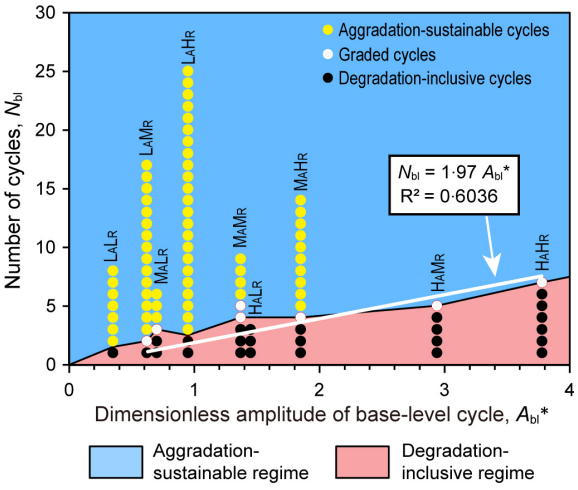


**Fig. 13.** Transition of the alluvial-shelf system from the degradation-inclusive phase to the aggradation-sustainable phase observed through the nine runs, showing a roughly linear relationship between dimensionless amplitude of base-level change ($A_{bl}$*) and the number of cycles elapsed ($N_{bl}$). Recognition of the two phases is based on whether or not global degradation happened during base-level fall. An implication here is that, given that a sufficient number of cycles elapsed (for example, $N_{bl}$ >> $2A_{bl}$*), the alluvial-shelf system can eventually attain an aggradation-sustainable state irrespective of how long and how many times base-level fall has been experienced. Note that the alluvial-shelf systems started to grow from the setting where no pre-existing deposit was in the basin. Degradation and aggradation mentioned in this figure are limited to the period during which the river-delta extended on top of the shelf. Degradation might take place when the delta has prograded beyond a higher relief shelf edge. See text for discussion.

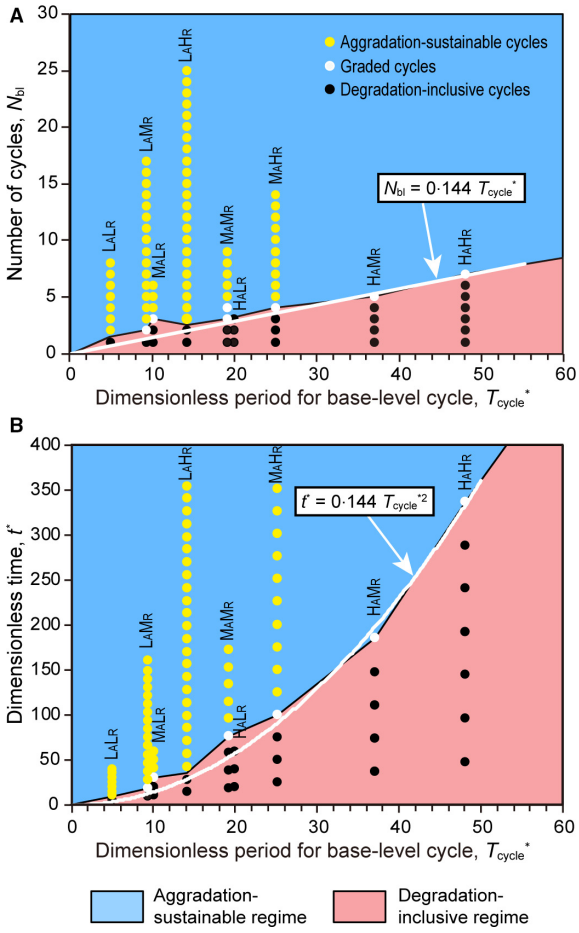


**Fig. 14.** Transition of the alluvial-shelf system from the degradation-inclusive phase to the aggradation-sustainable phase, in terms of dimensionless time. (A) The results clearly show that the number of cycles elapsed ($N_{bl}$) prior to the graded cycle is linearly proportional to the dimensionless period for base-level cycle ($T_{cycle}$*). (B) The results show that the time elapsed prior to the graded cycle (in dimensionless form $t_{trans}$*) is linearly proportional to the square of $T_{cycle}$*.

and thus need to experience a larger number of base-level cycles (Fig. 11D; also see comparable results from groups 1 and 4). The relationship between $N_{bl}$ and $A_{bl}$* presented in Eq. 7 is applicable to the scenario where an alluvial-shelf system grows from the very initial stage with no pre-existing strata. With the pre-existing deposit having a significantly large volume, the earlier stages of degradation-inclusive cycles might be supressed and even not occur.

By combining Eqs 5b and 7, the following relationship can be derived:

$$N_{bl} \sim \alpha T^*_{cycle} \tag{8}$$

The number of base-level cycles ($N_{bl}$) is also given by dividing the required time with the period of cycle:

$$N_{bl} = \frac{t^*_{trans}}{T^*_{cycle}} \tag{9}$$

where $t_{trans}$* is the dimensionless time required to elapse before the transition from the earlier degradation-inclusive to later aggradation-sustainable phase. Equation 8 is thus equivalent to Eq. 10:

$$t^*_{trans} \sim \alpha T^{*2}_{cycle} \tag{10}$$

Both Eqs 8 and 10 are supported by the experimental results (Fig. 14; $\alpha = 0.144$ as averaged

from all nine runs). Equations 8 and 10 are equivalent to Eq. 7, but can give interpretations in terms of time (Fig. 14). As noted above, a given period of base-level change (i.e. $T_{cycle}$) relative to the timescale (i.e. $\tau_{2D}$), i.e. $T_{cycle}^*$, controls how prominently the large-scale non-equilibrium response is manifested during the period. For the non-equilibrium responses (as typically seen in early stages) to vanish, the alluvial-shelf system is required to have a specific, large size that is obtained only after a particular number of cycles ($N_{bl}$) and thus a particular time interval elapsed (i.e. $t_{trans}^*$).

Equations 7, 8 and 10, derived from a 2D consideration in dip directions, may be extendable to 3D alluvial-shelf systems as well. In 3D sedimentary systems, sedimentological and tectonic processes can vary significantly in 3D directions (Posamentier & Allen, 1993; Wehr, 1993; Gawthorpe *et al.*, 1994; Ritchie *et al.*, 2004). For example, river flow does not usually cover all areas of a landscape at once, and channel networks may cause sediment deposition/erosion at high rates at particular places while some other places are starved of sediment. Stratigraphic information may not be equally stored along different dip-oriented sections of a 3D system, and elements of the stratigraphy may be recorded in some profiles while missed in others. Nevertheless, if sediment accumulation in a specific 2D profile of the 3D system can be approximated to be constant, the present 2D model will be applicable to this specific profile (Paola, 2000). In fact, a 3D system can be approximated as a succession of 2D slices (Paola, 2000), and 2D models can account for local 3D effects.

Suppose that a 3D system is divided into a number of slices of 2D sections and each 2D section represents $1/n$ of the 3D system. For simplification, considering that the sediment supply rate along a 2D section ($q_s$, per unit width) is $1/n$ of the rate supplied to the entire (full width) system, then Eqs 7, 8 and 10 may be modified as:

$$N_{bl} \sim 2nA_{bl}^* \quad (11)$$

$$N_{bl} \sim n\alpha T_{cycle}^* \quad (12)$$

$$t_{trans}^* \sim n\alpha T_{cycle}^{*2} \quad (13)$$

respectively.

Although the value of $n$ would greatly vary depending on individual natural systems, the relationships expressed by Eqs 11 to 13 might be retained. An implication from Eqs 7, 8 and 10 to 13 is that as long as the steady base-level cycles proceed, the alluvial-shelf system can eventually reach the aggradation-sustainable phase even though the base-level changes (falls, in particular) are of a very high rate and/or a very high amplitude.

## Application to natural systems

### *Natural alluvial-shelf systems growing under sea-level cycles*

Figures 13 and 14 provide an autostratigraphic implication for processes of real-world alluvial-shelf systems, which were constructed under nearly symmetrical cycles of relative sea-level changes but without the effect of subsidence (e.g. Sahagian *et al.*, 1996) or 3D morphodynamics (e.g. Straub & Foreman, 2018). During the icehouse periods, the sea level changed with a high $|R_{bl}|$ and a high $A_{bl}$, whereas during the greenhouse periods, both $|R_{bl}|$ and $A_{bl}$ were much lower (Miller *et al.*, 2005; Sømme *et al.*, 2009). As a result, $A_{bl}^*$ during the icehouse periods (for example, Pleistocene) could be dozens of times higher than that during the greenhouse periods (for example, late Cretaceous to early Palaeocene) according to Sømme *et al.* (2009). Thus, assuming symmetrical cycles with no subsidence or uplift, alluvial-shelf systems during greenhouse periods, rather than those during icehouse periods, were much more likely to transition into the aggradation-sustainable phase (Steel *et al.*, 2008).

The Pliocene–Quaternary succession of the shelf system off Rio de Janeiro State, northern Santos Basin (Fig. 15), might serve as a natural example to illustrate the autostratigraphic concepts presented above. Although there were no distinct feeder rivers during the Pliocene–Quaternary, small river networks on top of the strand plain might have provided an effective sediment supply to contribute to the shelf development during eustatic cycles (Reis *et al.*, 2013). The shelf system was constructed through stacking of transgressive–regressive stratigraphic units (possibly strand plain units), geometrically similar to the experimental alluvial-shelf system. In total, eight individual units were documented in the given stratigraphic profile, which were grouped into two distinctive stratigraphic sets: Sets I and II (Maia *et al.*, 2010; Reis *et al.*, 2013; Fig. 15A and B). Set I, which was stacked mostly during the Pliocene,

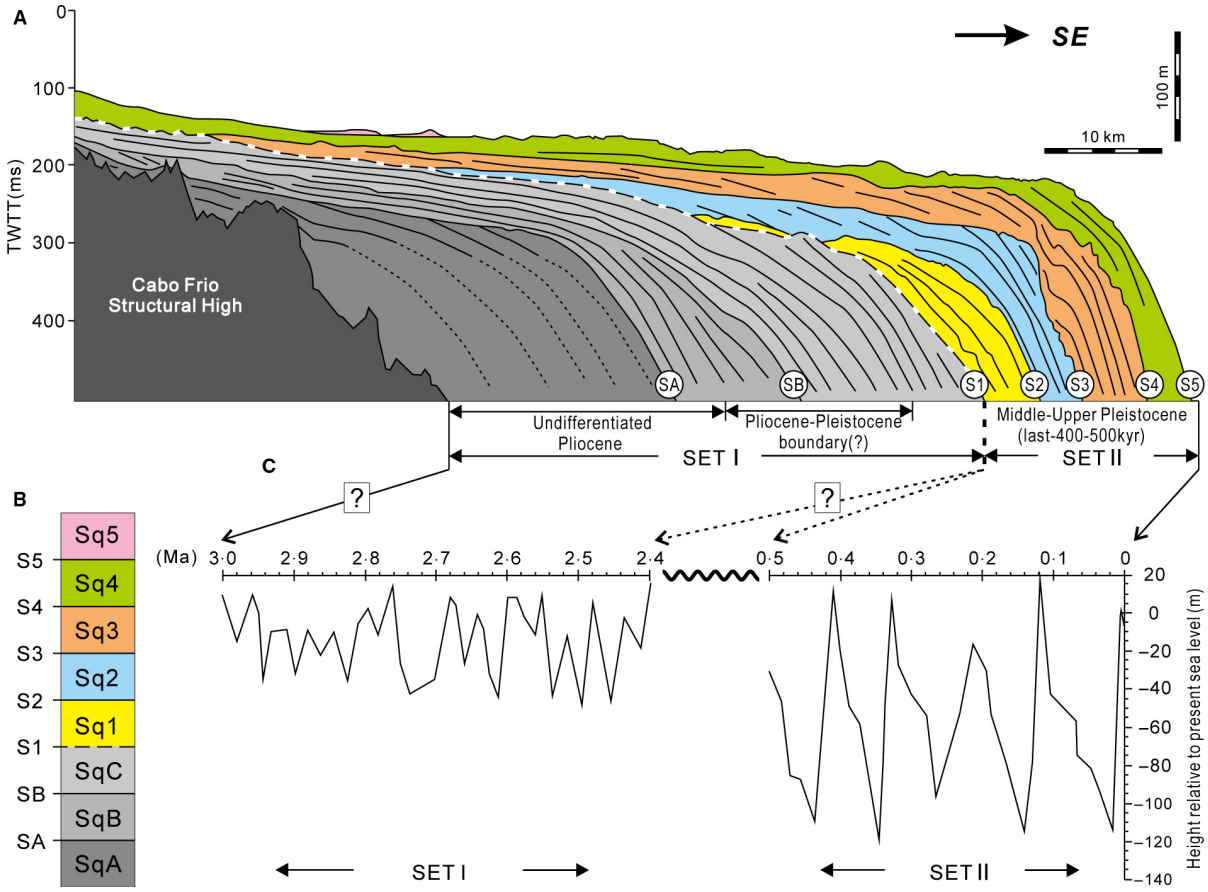


**Fig. 15.** Pliocene–Quaternary succession of the continental shelf off Rio de Janeiro State, northern Santos Basin, Brazil. (A) Line-drawing illustrating the internal seismic stratigraphical architecture. (B) Stratigraphic column showing subdivision of stratigraphic units. (C) Coeval approximated sea-level curve. (A) and (B) are modified from Reis *et al.* (2013); (C) is modified from Sømme *et al.* (2009).

consists of three stratigraphic units (SqA, SqB and SqC). Set II, made up of the other five stratigraphic units (Sq1, Sq2, Sq3, Sq4 and Sq5), was developed during the Pleistocene–Holocene (Maia *et al.*, 2010; Reis *et al.*, 2013; Fig. 15A and B). The coeval sea-level rising and lowering were almost symmetrical (Miller *et al.*, 2005; Sømme *et al.*, 2009; Fig. 15C).

Seismic stratigraphic analysis of the shelf system documents that Set I units possess aggradational-prone topsets having a smooth transition from the foreset, and Set II units (particularly Sq2 and Sq3), in contrast, lack topset components and are topped by seaward-dipping 'truncation' surfaces (Maia *et al.*, 2010). An existing interpretation attributes the aggradational component of Set I units to an increase in sediment supply rate and/or accommodation that allowed the preservation of the aggradational topset, while the lack of a topset component in the Set II units was due to a decrease in accommodation (Maia *et al.*, 2010).

The experimental results presented above can provide an alternative explanation in terms of intrinsic stratigraphic responses. A comparison of the stratigraphic column with the coeval sea-level curve (Fig. 15C) reveals that Set I appears to have developed with a lower amplitude ($A_{bl}$ ~ 30 m) and a lower rate ($|R_{bl}|$ ~ 1.83 m kyr$^{-1}$) of relative sea-level changes, while during the formation of Set II, $A_{bl}$ (*ca* 120 m) and $|R_{bl}|$ (*ca* 3.94 m kyr$^{-1}$) were much higher. By approximating a constant value of $q_s$ ~ 1.2 × 10$^4$ m$^2$ kyr$^{-1}$ along this particular section (by dividing the depositional area of Set II *ca* 6.0 × 10$^6$ m$^2$ with 500 kyr; Fig. 15A), $A_{bl}$* is calculated to

be *ca* $5 \times 10^{-3}$ for Set I and *ca* $4 \times 10^{-2}$ for Set II (Eqs 3a and 3b).

Equation 7 is here chosen to represent the application of the proportional relationships expressed in Eqs 7 to 10. Through Eq. 7, $N_{bl}$ values for Set I and Set II can be estimated separately. Before utilizing Eq. 7, $A_{bl}$* values for field scale ($A_{blF}$*) should be calibrated to the experimental scale ($A_{blE}$*). To achieve this, Eq. 7 is assumed to hold in natural systems by considering geometric similarities. As suggested from the discussion above, the effect of base-level amplitude on the stratigraphy of alluvial-shelf systems is dependent partly on the height of the system relative to the magnitude of amplitude. This, at least in part, affects the spatial extent of transgression ($L_{ts}$), initial alluvial length ($L_0$), and local and average slopes of the flooding surface ($\phi_{local}$ and $\phi_{avg}$, respectively). The subaerial height of the system is expressed as $\alpha\Lambda_{2D}$. Thus, the ratio of the base-level amplitude ($A_{bl}$) to $\alpha\Lambda_{2D}$ can affect the alluvial-shelf stratigraphy and be valid for both experimental and natural systems, i.e:

$$\frac{A_{blF}}{\alpha_F \Lambda_{2DF}} = \frac{A_{blE}}{\alpha_E \Lambda_{2DE}} \tag{14a}$$

where the subscripts 'F' and 'E' indicate values on the field and experimental scales, respectively. Equation 14a is reduced to:

$$\frac{A^*_{blF}}{A^*_{blE}} = \frac{\alpha_F}{\alpha_E} \tag{14b}$$

By adopting $\alpha_F \sim 0.002$, as measured from Fig. 15A, and $\alpha_E \sim 0.14$, as averaged from the experimental results (Table 2), $\alpha_F/\alpha_E$ in Eq. 14b is calculated as 1/70. As a result, $A_{blE}$* values for Set I and Set II are 0.35 and 2.66, respectively (Eqs 14a and 14b). According to Eq. 7, the $N_{bl}$ values for Set I and Set II are computed as 0.7 and 5.2, respectively. A lower $A_{bl}$* during the formation of Set I and a higher $A_{bl}$* during the formation of Set II would have favoured enhancing and suppressing the topset aggradation, respectively, although the effects brought about by the regional subsidence, 3D morphodynamics and grain-size effects are not considered in the $N_{bl}$ values.

### Effect of shelf edge relief

In the experiment, the base level always returned to the same position at the end of each cycle, i.e. 1 cm above the flume basement (Fig. 5J to R). This means that after each base-level rise (i.e. after the onset of non-deltaic transgression), a shelf edge just 1 cm above the basin basement (except for the first rise) was formed. An important point here is that this height was smaller than any of the $h_{set\_crt}$ values of the nine runs (Table 2). Modulated with the foreset slope ($\beta = 0.6$ to 0.7), the shelf margin slope is only approximately 1.43 to 1.67 cm in basinward width. During the latest stage of each base-level fall (except for the first base-level fall), the delta easily prograded beyond the low-relief shelf edge and then onto the horizontal basin floor. During this late-stage base-level fall, the basin floor slope ($\phi = 0$) was definitely gentler than the overlying alluvial slope. As a result, a sharp decrease in delta set thickness at the latest stage of each base-level fall existed (Figs 6 to 10). Therefore, in a strict sense, the system was aggradational at the end of each base-level fall when $h_{set} < h_{set\_crt}$ was inevitably realized.

Suppose that, owing to tectonic subsidence, the base level returns to a higher level at the end of each cycle so that the delta may be thicker than the critical value after it prograded beyond the shelf edge. In this case, regardless of whether a regressive delta prior to reaching the shelf edge is aggradational or degradational, degradation or global erosion would easily be triggered after the sea level drops to a level below the shelf edge. This fact is well acknowledged in existing stratigraphic models (Posamentier *et al.*, 1988, 1992; Posamentier & Vail, 1988; Blum & Törnqvist, 2000; Porębski & Steel, 2006; Burgess *et al.*, 2008; Bijkerk *et al.*, 2016). The validity of Figs 13 and 14 is limited to the setting where regressive deltas do not prograde beyond the shelf edge.

Additionally, even if the base-level cycles are in a symmetrical pattern (i.e. without tectonic effects), a higher shelf-edge relief might contribute to a delay in the transition of the shelf-transiting alluvial system from the earlier degradation-inclusive phase to the later aggradation-sustainable phase. This is because a higher shelf-edge relief or deeper basin floor tends to decline the expansion rate of the entire alluvial-shelf system (Gawthorpe *et al.*, 1994; Uličný *et al.*, 2002; Wang *et al.*, 2019a), whereby the slope condition of $\phi_{avg} \sim \alpha$ would be realized later than it would in the case where the shelf-edge relief is lower.

**Effect of long-term subsidence and uplift**

Possible effects of long-term tectonic subsidence and uplift are further considered. If tectonic subsidence or uplift is added to the aforementioned base-level scenario, it would function equivalently to a longer-term rising or falling component, respectively, whereby the relative sea-level cycles will be in an asymmetrical pattern. Assumptions adopted below are that: (i) the rates of tectonic subsidence and uplift are spatially uniform and much lower than those of base-level changes (i.e. $R_{bl}$); and, thus, (ii) the base-level rise and fall are not significantly accelerated or decelerated by tectonic activities such as the case where glacio-eustatic cycles superimpose on thermal subsiding passive margins. For simplification, non-uniform tectonism along the 'source to sink profile', which would result in both spatial and temporal variations in hinterland slope (i.e. $\gamma$) and basin slope (i.e. $\phi$) (e.g. Posamentier *et al.*, 1988; Kim *et al.*, 2006; Hoogendoorn *et al.*, 2008), is not considered.

*Effects of subsidence*

Tectonic subsidence can be relevant to autostratigraphic events, suggesting the possibility that the convergence of non-equilibrium responses to equilibrium responses is suppressed. Subsidence tends to raise the height of the shelf edge built by the delta at the end of each base-level fall (Porębski & Steel, 2006; Burgess *et al.*, 2008) and never attains the delta set thickness condition that $h_{set} \leq h_{set\_crt}$. Thus, with cycles proceeding under continuing subsidence, degradation would inevitably occur during base-level fall, at least in later cycles, only if the delta reaches the shelf-edge position. Such a scenario of base-level change has been adopted in recent experimental works performed by Li *et al.* (2016) and Yu *et al.* (2017). In their three-dimensional (3D) experiments, topset erosion was obvious and sustained during early, mid and late stages of 20 cycles, although this might be attributed partly to the 3D morphodynamic effect.

In the subsidence background, the alluvial length ($L$) may tend not to increase over cycles, because the large-scale rise (or subsidence) will inevitably force the system to undergo an overall process of shoreline autoretreat (Muto & Steel, 1992, 1997, 2002). In this sense, both allobreak and subsequent non-deltaic transgression will be less likely to occur than with symmetrical base-level cycles. Thus, the non-equilibrium responses are not likely to converge to the alternation of non-deltaic transgression for base-level rise and aggradational-deltaic regression for base-level fall. Degradation-free phases, as well as graded phases, are less likely attained as long as the subsidence continues. Although the alluvial-shelf system continues to grow, it tends to expand upward rather than basinward over a long horizontal distance, reflecting the enhanced effect of the rising trend of relative sea level.

*Effects of uplift*

Uplift also affects the non-equilibrium responses and their convergence. With long-term uplift of the basin (horizontal basement, initially), the shelf-edge position would be lowered with cycles, so that $h_{set} << h_{set\_crt}$, in general. As a result, the likelihood of alluvial degradation is supposed to decrease or may finally be nil with cycles continuing. Three-dimensional experimental works performed independently by Bijkerk *et al.* (2016) and Petter & Muto (2008) support this view. Bijkerk *et al.* (2016) found that when the delta prograded into a deeper water environment (i.e. a higher shelf edge), base-level fall was accompanied by significant alluvial degradation, whereas when the water depth was shallower (i.e. a lower shelf edge), alluvial degradation became less significant. When the water depth was sufficiently shallow (i.e. a sufficiently low shelf edge), base-level fall no longer caused alluvial degradation (Petter & Muto, 2008; Bijkerk *et al.*, 2016). Because a long-term fall (or uplift) contributes to lengthen the overall alluvial-shelf system, earlier episodes of erosion during the shelfal transition will never re-occur once they have disappeared.

Continuing uplift will eventually bring about autodetachment (Petter & Muto, 2008), after which the entire depositional system becomes purely alluvial and sustains aggradation that is independent of the base-level cycles. Definitely, the effects of base level and its changes can be much less significant with an uplifting trend than in the case of symmetrical base-level cycles. The convergence of the non-equilibrium responses to equilibrium responses can be realized, which is not in the form of alternation of non-deltaic transgression for base-level rise and aggradational-deltaic regression for base-level fall, but in a pattern that non-deltaic alluvial aggradation proceeds through the base-level cycles.

## CONCLUSIONS

An autostratigraphic model of an alluvial-shelf system growing with steady base-level cycles is suggested from a series of 2D experiments. In the experiments, base-level cycles adopted were of a symmetrical pattern that was characterized by constant amplitude ($A_{bl}$), constant rates of rise and fall ($|R_{bl}|$), and constant periods of rise and fall ($T_{cycle}$). The main points of the model are as follows:

**1** The alluvial-shelf system cannot retain non-equilibrium responses in the initial/early cycles, which, through continuing base-level cycles, eventually converge to equilibrium responses. This 'overall' non-equilibrium response towards the equilibrium responses is accompanied by the transition of regimes from a degradation-inclusive phase (early cycles) to an aggradation-sustainable phase (later cycles), reflecting the progressive growth of the alluvial-shelf system, which is accompanied by progressive reduction in the influence of the base-level changes. In the intermediate phase, the topset alluvial reaches can attain autogenic grade, which is transient and cannot be sustained over a large number of base-level cycles.

**2** The stratigraphic responses of the alluvial-shelf system and their changes through steady base-level cycles are closely related to the progressive increase in the alluvial length and the progressive decrease in the delta set thickness. Both reflect the progressive spatial expansion of the system. For the system growing into the transitional grade phase with an initial condition of zero sediment accumulation, the preliminary number ($N_{bl}$) or duration ($t_{trans}{}^{*}$; in dimensionless form) of base-level cycles is linearly proportional to the dimensionless amplitude ($A_{bl}{}^{*} = A_{bl}/\Lambda_{2D}$; $\Lambda_{2D}$ is the 2D autostratigraphic length scale) or the square of the dimensionless cycle period ($T_{cycle}{}^{*2}$, $T_{cycle}{}^{*} = T_{cycle}/\tau_{2D}$; $\tau_{2D}$ is the 2D autostratigraphic time scale), respectively. Thus, as long as the steady base-level cycles proceed, the alluvial-shelf system eventually reaches the aggradation-sustainable phase, regardless of how fast the base-level changes with any high amplitude.

**3** Long-term subsidence or uplift, while steady base-level cycles in a symmetrical pattern proceed, can affect the non-equilibrium responses and their convergence to the equilibrium responses. Subsidence will function to enhance the effect of base-level changes and thus sustain the non-equilibrium response. In contrast, uplift will function to reduce and eventually cancel the effect of base-level changes and cause an earlier attainment of equilibrium responses that are characterized by sustained non-deltaic alluvial aggradation. Paradoxically enough, subsidence and uplift during base-level fall will tend to make the feeder alluvial river degrade and aggrade, respectively.

**4** In light of the present experimental verification, the recognition of the autostratigraphic responses and their changes through base-level (or relative sea level) cycles might be useful to make further refinements to existing sequence stratigraphic models, which have been developed without a sufficient appreciation of the effect of the progressive growth and hysteresis of the system.

## ACKNOWLEDGEMENTS

This study was supported by National Natural Science Foundation of China (No. 41702104, 41872113), a postdoctoral fellowship in Japan Society for the Promotion of Science (JSPS) to JW. TM appreciates financial support by the Japan Society for the Promotion of Science (KAKENHI 17F17031, 18K03785). This work also benefited from National Science and Technology Major Project (2017ZX05009-002), Science Foundation of China University of Petroleum, Beijing (No. 2462020BJRC002, 2462020YXZZ020) and PetroChina Innovation Foundation (2018D-5007-0102), which supported JW to continue the research during 2019 and 2020. The authors have no conflict of interest to declare. We sincerely thank Jesse Pisel, Peter Burgess and Kyle Straub for their constructive comments and suggestions provided to early versions of the manuscript.

## DATA AVAILABILITY STATEMENT

The data that support the findings of this study are available from the corresponding author upon reasonable request.

## NOMENCLATURE

| Symbol | Meaning | Dimensions (L, length; T, time; 1, dimensionless) |
|---|---|---|
| $A_{bl}$ | Amplitude of base-level change | L |
| $A_{bl}$* | Dimensionless amplitude of base-level change | 1 |
| $A_{blE}$ | $A_{bl}$ value in experimental scale | L |
| $A_{blE}$* | $A_{bl}$* value in experimental scale | 1 |
| $A_{blF}$ | $A_{bl}$ value in field scale | L |
| $A_{blF}$* | $A_{bl}$* value in field scale | 1 |
| $h_{agg\_blr}$ | Aggradational thickness of topset during base-level rise | L |
| $h_{set}$ | Set thickness of deltaic system | L |
| $h_{set}$* | Dimensionless set thickness of deltaic system | 1 |
| $h_{set\_crt}$ | Critical set thickness of deltaic system at autogenic grade | L |
| $h_{set\_crt}$* | Dimensionless critical set thickness of deltaic system at autogenic grade | 1 |
| $h_{set\_max}$ | Maximum set thickness of deltaic system | L |
| $h_{set\_max}$* | Dimensionless maximum set thickness of deltaic system | 1 |
| $I_{ts}$ | Transgressive ratio | 1 |
| $L$ | Alluvial length of river | L |
| $L$* | Dimensionless alluvial length of river | 1 |
| $L_0$ | Initial alluvial length of river prior to base-level rise | L |
| $L_0$* | Dimensionless initial alluvial length of river prior to base-level rise | 1 |
| $L_{crt}$ | Critical alluvial length of river | L |
| $L_{crt}$* | Dimensionless critical alluvial length of river | 1 |
| $L_{final}$ | Final alluvial length of river after base-level rise | L |
| $L_{final}$* | Dimensionless final alluvial length of river after base-level rise | 1 |
| $L_{system}$ | Horizontal length of entire depositional system | L |
| $L_{system}$* | Dimensionless horizontal length of entire depositional system | 1 |
| $L_{ts}$ | Horizontal length of maximum flooding surfaces | L |
| $L_{ts}$* | Dimensionless horizontal length of maximum flooding surfaces | 1 |
| $n$ | Divisor that slices a 3D system into a number of 2D sections | 1 |
| $N_{bl}$ | Number of base-level cycles | 1 |
| $q_s$ | Sediment supply rate per unit width | $L^2 \cdot T^{-1}$ |
| $q_w$ | Water supply rate per unit width | $L^2 \cdot T^{-1}$ |
| $R_{bl}$ | Rate of base-level change; $R_{bl} > 0$ for base-level rise; $R_{bl} < 0$ for base-level fall | $L \cdot T^{-1}$ |
| $T$ | Time elapsed | T |
| $t$* | Dimensionless time elapsed | 1 |
| $t_{trans}$* | Dimensionless time needed to elapse before the transition from the early degradation-inclusive to later aggradation-sustainable phase | 1 |

| Symbol | Meaning | Dimensions (L, length; T, time; 1, dimensionless) |
|---|---|---|
| $T_{bl}$ | Period of base-level change | T |
| $T_{bl}$* | Dimensionless period of base-level change | 1 |
| $T_{cycle}$ | Period of base-level cycle including a rise and a following fall | T |
| $T_{cycle}$* | Dimensionless period of base-level cycle including a rise and a following fall | 1 |
| $x$ | Horizontal distance along the direction of mean sediment flux | L |
| $x$* | Dimensionless horizontal distance along the direction of mean sediment flux | 1 |
| $X_{flume}$* | Dimensionless flume basement length | 1 |
| $z$ | Vertical upward distance | L |
| $z$* | Dimensionless vertical upward distance | 1 |
| $Z_{flume}$* | Dimensionless flume depth | 1 |
| $\alpha$ | Alluvial slope in tangent | 1 |
| $\alpha_E$ | Alluvial slope in tangent for experimental scale | 1 |
| $\alpha_F$ | Alluvial slope in tangent for field scale | 1 |
| $\beta$ | Foreset slope in tangent | 1 |
| $\gamma$ | Hinterland slope in tangent | 1 |
| $\phi$ | General basin floor slope in tangent | 1 |
| $\phi_{avg}$ | Average basin floor or shelf slope from shelf edge to shoreline, in tangent | 1 |
| $\phi_{local}$ | Local slope of the shelf just basinward of the shoreline | 1 |
| $\Lambda_{2D}$ | Autostratigraphic length scale in two dimensions | L |
| $\Lambda_{2DE}$ | $\Lambda_{2D}$ value in experimental scale | L |
| $\Lambda_{2DF}$ | $\Lambda_{2D}$ value in field scale | L |
| $\tau_{2D}$ | Autostratigraphic timescale in two dimensions | T |

## REFERENCES


**Bijkerk, J.F.**, **Eggenhuisen, J.T.**, **Kane, I.A.**, **Meijer, N.**, **Waters, C.N.**, **Wignall, P.B.** and **McCaffrey, W.D.** (2016) Fluvio-marine sediment partitioning as a function of basin water depth. *J. Sediment. Res.*, **86**, 217–235.

**Blom, A.**, **Viparelli, E.** and **Chavarrías, V.** (2016) The graded alluvial river: Profile concavity and downstream fining. *Geophys. Res. Lett.*, **43**, 6285–6293.

**Blum, M.D.** and **Törnqvist, T.E.** (2000) Fluvial responses to climate and sea-level change: a review and look forward. *Sedimentology*, **47**, 2–48.

**Burgess, P.M.** and **Allen, P.A.** (1996) A forward-modelling analysis of the controls on sequence stratigraphical geometries. *Geol. Soc. London Spec. Pub.*, **103**(1), 9–24.

**Burgess, P.M.** and **Prince, G.D.** (2015) Non-unique stratal geometries: implications for sequence stratigraphic interpretations. *Basin Res.*, **27**, 351–365.

**Burgess, P.M.**, **Steel, R.J.** and **Granjeon, D.** (2008) Stratigraphic forward modeling of basin-margin clinoform systems: implications for controls on topset and shelf width and timing of formation of shelf-edge deltas. In: *Recent Advances in Models of Siliciclastic Shallow-Marine Stratigraphy* (Eds Hampson, G.J., Steel, R.J., Burgess, P.M. and Dalrymple, R.W.), *SEPM Spec. Publ.*, **90**, 35–45.

**Catuneanu, O.**, **Abreu, V.**, **Bhattacharya, J.P.**, **Blum, M.D.**, **Dalrymple, R.W.**, **Eriksson, P.G.**, **Fielding, C.R.**, **Fisher, W.L.**, **Galloway, W.E.**, **Gibling, M.R.**, **Giles, K.A.**, **Holbrook, J.M.**, **Jordan, R.**, **Kendall, C.G.S.C.**, **Macurda, B.**, **Martinsen, O.J.**, **Miall, A.D.**, **Neal, J.E.**, **Nummedal, D.**, **Pomar, L.**, **Posamentier, H.W.**, **Pratt, B.R.**, **Sarg, J.F.**, **Shanley, K.W.**, **Steel, R.J.**, **Strasser, A.**, **Tucker, M.E.** and **Winker, C.** (2009) Toward the standardization of sequence stratigraphy. *Earth Sci. Rev.*, **92**, 1–33.

**Csato, I.**, **Catuneanu, O.** and **Granjeon, D.** (2014) Millennial-scale sequence stratigraphy: numerical simulation with Dionisos. *J. Sediment. Res.*, **84**, 394–406.

**Embry, A.F.** and **Johannessen, E.P.** (1993) T-R sequence stratigraphy, facies analysis and reservoir distribution in the uppermost Triassic-Lower Jurassic succession, western Sverdrup Basin, Arctic Canada. In: *Norwegian Petroleum Society Special Publications* (Eds Vorren, T.O., Bergsager, E., Dahl-Stamnes, Ø.A., Holter, E., Johansen, B., Lie, E. and Lund, T.B.), pp. 121–146. Amsterdam: Elsevier.

**Galloway, W.E.** (1989) Genetic stratigraphic sequences in basin analysis I: architecture and genesis of flooding-surface bounded depositional units. *AAPG Bulletin*, **73**, 125–142.

**Gawthorpe, R.L.**, **Fraser, A.J.** and **Collier, R.E.L.** (1994) Sequence stratigraphy in active extensional basins: Implications for the interpretation of ancient basin-fills. *Mar. Pet. Geol.*, **11**, 642–658.

**Hajek, E.A.** and **Straub, K.M.** (2017) Autogenic sedimentation in clastic stratigraphy. *Annu. Rev. Earth Planet. Sci.*, **45**, 681–709.

**Helland-Hansen, W.**, **Steel, R.J.** and **Sømme, T.O.** (2012) Shelf genesis revisited. *J. Sediment. Res.*, **82**, 133–148.

**Hoogendoorn, R.M.**, **Overeem, I.** and **Storms, J.E.A.** (2008) Process-response modelling of fluvio-deltaic stratigraphy. *Comput. Geosci.*, **34**, 1394–1416.

**Jervey, M.T.** (1988) Quantitative geological modeling of siliciclastic rock sequences and their seismic expression. In: *Sea-Level Changes: An Integrated Approach* (Eds Wilgus, C.K., Hastings, B.S., Kendall, C.G.S.C., Posamentier, H.W., Ross, C.A. and van Wagoner, J.C.), *SEPM Spec. Publ.*, **42**, 47–69.

**Kim, W.** and **Muto, T.** (2007) Autogenic response of alluvial-bedrock transition to base-level variation: Experiment and theory. *J. Geophys. Res.*, **112**, F03S14.

**Kim, W.**, **Paola, C.**, **Swenson, J.B.** and **Voller, V.T.** (2006) Shoreline response to autogenic processes of sediment storage and release in the fluvial system. *J. Geophys. Res.*, **111**, F04013.

**Kim, W.**, **Petter, A.**, **Straub, K.** and **Mohrig, D.** (2014) Investigating the autogenic process response to allogenic forcing: experimental geomorphology and stratigraphy. In: *From Depositional Systems to Sedimentary Successions on the Norwegian Continental Margin* (Eds Martinius, A.W., Ravnås, R., Howell, J.A., Steel, R.J. and Wonham, J.P.), *IAS Spec. Publ.*, **46**, 127–138.

**Li, Q.**, **Yu, L.** and **Straub, K.M.** (2016) Storage thresholds for relative sea-level signals in the stratigraphic record. *Geology*, **44**, 179–182.

**Maia, R.M.D.C.**, **Reis, A.T.D.**, **Alves, E.D.C.**, **Silva, C.G.**, **Guerra, J.V.**, **Gorini, C.**, **Silva, A.** and **Arantes-Oliveira, R.** (2010) Architecture and stratigraphic framework of shelf sedimentary systems off Rio de Janeiro state, Northern Santos Basin-Brazil. *Brazilian J. Oceanogr.*, **58**, 15–29.

**Martin, J.**, **Paola, C.**, **Abreu, V.**, **Neal, J.** and **Sheets, B.** (2009) Sequence stratigraphy of experimental strata under known conditions of differential subsidence and variable base level. *AAPG Bulletin*, **93**, 503–533.

**Miller, K.G.**, **Kominz, M.A.**, **Browning, J.V.**, **Wright, J.D.**, **Mountain, G.S.**, **Katz, M.E.**, **Sugarman, P.J.**, **Cramer, B.S.**, **Christie-Blick, N.** and **Pekar, S.F.** (2005) The Phanerozoic record of global sea-level change. *Science*, **310**, 1293–1298.

**Muto, T.** (2001) Shoreline autoretreat substantiated in flume experiments. *J. Sediment. Res.*, **71**, 246–254.

**Muto, T.**, **Furubayashi, R.**, **Tomer, A.**, **Sato, T.**, **Kim, W.**, **Naruse, H.** and **Parker, G.** (2016a) Planform evolution of deltas with graded alluvial topsets: insights from three-dimensional tank experiments, geometric considerations and field applications. *Sedimentology*, **63**, 2158–2189.

**Muto, T.** and **Steel, R.J.** (1992) Retreat of the front in a prograding delta. *Geology*, **20**, 967–970.

**Muto, T.** and **Steel, R.J.** (1997) Principles of regression and transgression: the nature of the interplay between accommodation and sediment supply. *J. Sediment. Res.*, **67**, 994–1000.

**Muto, T.** and **Steel, R.J.** (2001) Autostepping during the transgressive growth of deltas: Results from flume experiments. *Geology*, **29**, 771–774.

**Muto, T.** and **Steel, R.J.** (2002) In defense of shelf-edge delta development during falling and lowstand of relative sea level. *J. Geol.*, **110**, 421–436.

**Muto, T.** and **Steel, R.J.** (2004) Autogenic response of fluvial deltas to steady sea-level fall: implications from flume-tank experiments. *Geology*, **32**, 401–404.

**Muto, T.** and **Steel, R.J.** (2014) The autostratigraphic view of responses of river deltas to external forcing: a review of the concepts. *IAS Spec. Publ.*, **46**, 139–148.

**Muto, T.**, **Steel, R.J.** and **Burgess, P.** (2016b) Contributions to sequence stratigraphy from analogue and numerical experiments. *J. Geol. Soc.*, **173**, 837–844.

**Muto, T.**, **Steel, R.J.** and **Swenson, J.B.** (2007) Autostratigraphy: a framework norm for genetic stratigraphy. *J. Sediment. Res.*, **77**, 2–12.

**Muto, T.** and **Swenson, J.B.** (2005) Large-scale fluvial grade as a nonequilibrium state in linked depositional systems: theory and experiment. *J. Geophys. Res.*, **110**, F03002.

**Muto, T.** and **Swenson, J.B.** (2006) Autogenic attainment of large-scale alluvial grade with steady sea-level fall: an analog tank-flume experiment. *Geology*, **34**, 161–164.

**Nijhuis, A.G.**, **Edmonds, D.A.**, **Caldwell, R.L.**, **Cederberg, J.A.**, **Slingerland, R.L.**, **Best, J.L.**, **Parsons, D.R.** and **Robinson, R.A.J.** (2015) Fluvio-deltaic avulsions during relative sea-level fall. *Geology*, **43**, 719–722.

**Nittrouer, J.**, **Shaw, J.**, **Lamb, M.P.** and **Mohrig, D.** (2012) Spatial and temporal trends for water-flow velocity and bed-material sediment transport in the lower Mississippi River. *GSA Bulletin*, **124**, 400–414.

**Paola, C.** (2000) Quantitative models of sedimentary basin filling. *Sedimentology*, **47**, 121–178.

**Paola, C.** (2016) A mind of their own: recent advances in autogenic dynamics in rivers and deltas. In: *Autogenic Dynamics and Self-organization in Sedimentary Systems* (Eds Budd, D.A., Hajek, E.A. and Purkis, S.J.), *SEPM Spec. Publ.*, **106**, 5–17.

**Paola, C.**, **Heller, P.L.** and **Angevine, C.L.** (1992) The large-scale dynamics of grain-size variation in alluvial basins, 1: theory. *Basin Res*, **4**, 73–90.

**Paola, C.**, **Mullin, J.**, **Ellis, C.**, **Mohrig, D.C.**, **Swenson, J.B.**, **Parker, G.**, **Hickson, T.**, **Heller, P.L.**, **Pratson, L.**, **Syvitski, J.**, **Sheets, B.** and **Strong, N.** (2001) Experimental stratigraphy. *GSA Today*, **11**, 4–9.

**Patruno, S.** and **Helland-Hansen, W.** (2018) Clinoforms and clinoform systems: Review and dynamic classification scheme for shorelines, subaqueous deltas, shelf edges and continental margins. *Earth Sci. Rev.*, **185**, 202–233.

**Petter, A.L.** and **Muto, T.** (2008) Sustained alluvial aggradation and autogenic detachment of the alluvial river from the shoreline in response to steady fall of relative sea level. *J. Sediment. Res.*, **78**, 98–111.

**Porębski, S.J.** and **Steel, R.J.** (2006) Deltas and sea-level change. *J. Sediment. Res.*, **76**, 390–403.

**Posamentier, H.W.** and **Allen, G.P.** (1993) Variability of the sequence stratigraphic model: effects of local basin factors. *Sed. Geol.*, **86**, 91–109.

**Posamentier, H.W.**, **Allen, G.P.**, **James, D.P.** and **Tesson, M.** (1992) Forced regressions in a sequence stratigraphic framework: concepts, examples, and exploration significance (1). *AAPG Bulletin*, **76**, 1687–1709.

**Posamentier, H.W.**, **Jervey, M.T.** and **Vail, P.R.** (1988). Eustatic controls on clastic deposition I—conceptual framework. In: *Sea-Level Changes: An Integrated Approach* (Eds Wilgus, C.K., Hastings, B.S., Kendall, C.G.S.C., Posamentier, H.W., Ross, C.A. and van Wagoner, J.C.), *SEPM Spec. Publ.*, **42**, 109–124.

**Posamentier, H.W.** and **Vail, P.R.** (1988) Eustatic controls on clastic deposition II—sequence and system tracts models. In: *Sea-Level Changes: An Integrated Approach* (Eds Wilgus, C.K., Hastings, B.S., Kendall, C.G.S.C., Posamentier, H.W., Ross, C.A. and van Wagoner, J.C.), *SEPM Spec. Publ.*, **42**, 125–154.

**Reis, A.T.**, **Maia, R.M.C.**, **Silva, C.G.**, **Rabineau, M.**, **Guerra, J.V.**, **Gorini, C.**, **Ayres, A.**, **Arantes-Oliveira, R.**, **Benabdellouahed, M.**, **Simões, I.** and **Tardin, R.** (2013) Origin of step-like and lobate seafloor features along the continental shelf off Rio de Janeiro State, Santos basin-Brazil. *Geomorphology*, **203**, 25–45.

**Ritchie, B.D.**, **Gawthorpe, R.L.** and **Hardy, S.** (2004) Three-dimensional numerical modeling of deltaic depositional sequences 1: influence of the rate and magnitude of sea-level change. *J. Sediment. Res.*, **74**, 203–220.

**Sahagian, D.**, **Pinous, O.**, **Olferiev, A.** and **Zakharov, V.** (1996) Eustatic curve for the Middle Jurassic-Cretaceous based on Russian platform and Siberian stratigraphy: zonal resolution. *AAPG Bulletin*, **80**, 1433–1458.

**Sømme, T.O.**, **Helland-Hansen, W.** and **Granjeon, D.** (2009) Impact of eustatic amplitude variations on shelf morphology, sediment dispersal, and sequence stratigraphic interpretation: icehouse versus greenhouse systems. *Geology*, **37**, 587–590.

**Steel, R.J.**, **Carvajal, C.**, **Petter, A.L.** and **Uroza, C.** (2008) Shelf and shelf-margin growth in scenarios of rising and falling sea level. In: *Recent Advances in Models of Siliciclastic Shallow-Marine Stratigraphy* (Eds Hampson, G.J., Steel, R.J., Burgess, P.M. and Dalrymple, R.W.), *SEPM Spec. Publ.*, **90**, 47–71.

**Straub, K.M.** (2019) Morphodynamics and Stratigraphic Architecture of Shelf-Edge Deltas Subject to Constant vs. Dynamic Environmental Forcings: A Laboratory Study. *Front. Earth Sci.*, **7**, 121.

**Straub, K.M.** and **Foreman, B.Z.** (2018) Geomorphic stasis and spatiotemporal scales of stratigraphic completeness. *Geology*, **46**, 311–314.

**Swenson, J.B.** (2005) Fluviodeltaic response to sea level perturbations: amplitude and timing of shoreline translation and coastal onlap. *J. Geophys. Res.*, **110**, F03007.

**Swenson, J.B.** and **Muto, T.** (2007) Response of coastal plain rivers to falling relative sea-level: allogenic controls on the aggradational phase. *Sedimentology*, **54**, 207–221.

**Tomer, A.** and **Muto, T.** (2010) Emergence and drowning of fluviodeltaic systems during steady rise of sea level: implication from geometrical modeling and tank experiments. *J. Sedimentol. Soc. Japan*, **69**, 63–72.

**Tomer, A.**, **Muto, T.** and **Kim, W.** (2011) Autogenic hiatus in fluviodeltaic successions: geometrical modeling and physical experiments. *J. Sediment. Res.*, **81**, 207–217.

**Uličný, D.**, **Nichols, G.** and **Waltham, D.** (2002) Role of initial depth at basin margins in sequence architecture: Field examples and computer models. *Basin Res.*, **14**, 347–360.

**Van Heijst, M.W.I.M.** and **Postma, G.** (2001) Fluvial response to sea-level changes: a quantitative analogue, experimental approach. *Basin Res.*, **13**, 269–292.

**Van Wagoner, J.C.**, **Posamentier, H.W.**, **Mitchum, R.M.**, **Vail, P.R.**, **Sarg, J.F.**, **Loutit, T.S.** and **Hardenbol, J.** (1988) An overview of the fundamentals of sequence stratigraphy and key definitions. In: *Sea-Level Changes: An Integrated Approach* (Eds Wilgus, C.K., Hastings, B.S., Kendall, C.G.S.C., Posamentier, H.W., Ross, C.A. and van Wagoner, J.C.), *SEPM Spec. Publ.*, **42**, 39–45.

**Wang, J.**, **Muto, T.**, **Urata, K.**, **Sato, T.** and **Naruse, H.** (2019a) Morphodynamics of River Deltas in Response to Different Basin Water Depths: An Experimental Examination of the Grade Index Model. *Geophys. Res. Lett.*, **46**, 5265–5273.

**Wang, J.**, **Tamura, T.** and **Muto, T.** (2019b) Construction and destruction of an autogenic grade system: The late Holocene Mekong River delta. *Geology*, **47**(7), 669–672.

**Wehr, F.L.** (1993) Effects of variation in subsidence and sediment supply on parasequence stacking patterns. In: *Siliciclastic Sequence Stratigraphy—Recent Developments and Applications* (Eds Weimer, P. and Posamentier, H.W.), *Am. Assoc. Petrol. Geol., Memoir.*, **58**, 369–379.

**Yu, L.**, **Li, Q.** and **Straub, K.M.** (2017) Scaling the response of deltas to relative-sea-level cycles by autogenic space and time scales: A laboratory study. *J. Sediment. Res.*, **87**, 817–837.

*Manuscript received 10 September 2018; revision 14 June 2020; revision accepted 25 July 2020*